Journal of the Geological Survey of Brazil

Post-collisional 1.75 Ga mantle-derived felsic magmatism in the Cauaburi Orogeny, NW Amazon Craton, Brazil

Marcelo E. Almeida[1*], Moacir J. B. Macambira[2], Túlio Amós de Araújo Mendes[3], João Orestes S. dos Santos[4]

[1] Geological Survey of Brazil-CPRM, Av. Pasteur, 404, Urca, CEP 22290-255, Rio de Janeiro, Brazil
[2] Institute of Geosciences, Federal University of Pará, Rua Augusto Corrêa s/n, Guamá, CEP 66075-110, Belém, Pará, Brazil
[3] Geological Survey of Brazil-CPRM, Av. André Araújo 2160, Aleixo, CEP 69060-000, Manaus, Brazil
[4] University of Western Australia, Perth, Australia

Abstract

In the Amazon NW craton, ~1.75 Ga granites are commonly found inboard (eastern) the Cauaburi Magmatic Arc (1.81-1.76 Ga, flare-up phase), generated during the final stages of retreat of the arc westward, a process that lasted approximately 80 million years. This magmatism is more abundant in the Northeastern Domain (Marauiá and Marié-Mirim suites), exhibiting higher volumes in more exhumed areas and elongated shapes suggesting structural control (Imeri Terrain). These granites are locally deformed in shear zones under high strain rates (D_{n+2}) and metamorphism with greenschist to epidote-amphibolite facies conditions (K´Mudku Shear Belt). The granites in this region are characterized as peralkaline to peraluminous, ferroan, and alkalic to calc-alkaline, with chemical signatures consistent with A-type magmas. In the Southwestern Domain (Tiquié Suite), these granites occur in smaller volumes, with subcircular shapes and contemporaneous volcanism (Cachoeira do Machado Formation), suggesting emplacement on higher crustal levels (Uaupés Terrain). They are also deformed under lower strain rates (D_{n+3}?) and low greenschist facies conditions (Traíra Shear Belt). These granites are metaluminous, ferroan to magnesian, and alkalic-calcic, showing Nb-Ta negative anomalies, suggesting transitional characteristics between I-type and A-type granites ("ambiguous" granites). All of these granitic suites are enriched in SiO_2 (70-76%) and high-field strength elements (HFSE), contain dissolved OH–F-bearing fluids, and exhibit a range of magma oxidation states, from reduced in the Marié-Mirim Suite to oxidized in the Marauiá and Tiquié suites. The magmas are derived from a depleted source, or sources containing an important mantle input (εNd +2.27 to +0.92), with temperature models suggesting ranges from 1205°C to 1085°C. The granite's origins probably involve partial melting of lower crustal quartz feldspathic igneous or charnockite sources (Tiquié and Marauiá suites) and differentiation of tholeiitic mafic sources with low contributions of crustal sources (Marié-Mirim Suite), showing metallic fertility mineral potential for Sn, Ta, Nb and probably other rare metals and gemstones. These granites may have been generated from a model based on a late-orogenic magmatism (post-collisional), arc-related, associated with extensional tectonics, probably produced by underplating in a back-arc setting, or during the gravitational collapse of the Cauaburi orogen (post-1.78 Ga), involving mantle-derived magmas uprising and partial melting with low crustal sources interactions.

Article Information

Publication type: Research Papers
Received 26 August 2023
Accepted 8 October 2023
Online pub. 16 October 2023
Editor: Fabricio Caxito

Keywords:
Rio Negro-Juruena Province,
Cauaburi Orogen,
A-type Granites,
Underplating,
Amazonian Craton

*Corresponding author
Marcelo Esteves Almeida
E-mail address: marcelo.esteves@sgb.gov.br

1. Introduction

A wide range of geodynamic settings is reported for arc magmatism (e.g. Pirajno and Santosh 2015, Santosh et al. 2020, Chapman et al. 2021), which provides valuable insights into crust-mantle interaction during crustal growth (Hildreth and Moorbath 1988, Cawood and Hawkesworth 2015, Hawkesworth et al. 2016). Granitoids are commonly the dominant igneous rocks in preserved convergent margins, and their lithogeochemistry and isotopic compositions contribute to clarifying for example the mantle/crustal contribution in their genesis (e.g. Bonin et al. 2020).

This is particularly true for arc-related A-type granites where there is little consensus on the origin of this type of granites, despite their widespread global occurrence (Frost and Frost 2011, 2013, Bonin et al. 2020, Janoušek et al. 2020, Johansson 2023). Originally, A-type granites were defined as occurring in stable continental and rift zones, and classified

ISSN: 2595-1939
https://doi.org/10.29396/jgsb.2023.v6.n3.1
Open access at https://jgsb.cprm.gov.br/index.php/journal

as anorogenic granites (Loiselle and Wones 1979). This definition was later expanded to include all high-temperature (hypersolvus) granites emplaced in within-plate or post-collisional settings (e.g. Eby 1990, 1992).

Generally, ferroan or high-silica A-type granites are considered to have high alkalis, FeO_T, total contents of high field strength elements (HFSE), and rare earth elements (REEs), including high Ga/Al and Fe/Mg ratios (e.g. Bonin et al. 2020). Frost and Frost (2011) suggested abandoning the term A-type, proposing a classification scheme where these granites plot dominantly in the ferroan field (or high-silica granites). Despite this controversy, this typology is still widely used to classify the chemical signature of granites, recognizing that they can form in a variety of geodynamic settings (e.g. Bonin et al. 2020, Janoušek et al. 2020).

In general, A-type suites are generated from (1) crystallization of a parental mafic end-member derived from a mantle with different levels of crustal contamination or (2) crustal anatexis caused by underplating of a mantle-derived mafic magma (e.g. Frost and Frost 2011). In the first model, the chemical signature is ascribed to variations in the composition of the primitive basaltic magma, including the mechanism(s) that control fractionation (T, P, H_2O contents, redox state, etc.). On the other hand, the compositional differences in the second model are attributed to different sources and melt conditions (Bonin 2007).

Granites emplaced in the final stages of the Cauaburi Orogeny (1.81-1.76 Ga) are characterized by SiO_2-rich and A-type chemical signatures (Almeida 1997), hosting Sn and Nb-Ta mineralizations and gemstones (Almeida et al. 2000). This paper presents geology, petrography, zircon geochronology (single Pb-evaporation), multi-elemental lithogeochemisty, and Sm-Nd isotopic compositions for A-type granitoid rocks (and related rocks) of the Cauaburi Orogen, NW Amazon, in Western Magmatic Belt of Supercontinent Columbia. The data from the ca. 1750 Ma magmatic event provides insight into the contribution of juvenile x recycled material in the production of A-type magmas during the final stages of the Columbia assembly and the implications of the mineral potential associated with these intrusions. This research aims to discuss a petrological model for these granitoids and their importance in the crustal evolution of the Rio Negro Province.

2. Regional Geology

Located in the northwestern of the Amazon Craton (Guiana Shield), northern sector of the Rio Negro-Juruena (or Rio Negro) Province (**Figure 1**), the studied area was historically investigated from a regional point-of-view, including its geological, geochemical and geochronological aspects (e.g. Amaral 1974, Tassinari 1981, Tassinari et al. 1996, Tassinari and Macambira 1999, 2004, Dall'Agnol and Macambira 1992, Almeida and Larizzatti 1996a,b, Almeida et al. 2000, 2011, 2022, Santos et al. 2000, 2006a,b, Bizzi et al. 2004, Reis et al. 2006, Carneiro et al. 2017, Veras et al. 2018).The low density of geological data and the heterogeneous distribution of geochemical-isotopic data are reflected in the contrasting geodynamic models (e.g. Cordani et al. 1979, Teixeira et al. 1989, Tassinari and Macambira 2004, Macambira et al. 2020), making further studies necessary to improve or modify them. The main crustal evolutionary models for the Amazon craton suggest in a general sense that several Paleoproterozoic to Mesoproterozoic orogenic belts (e.g. Transamazon/Maroni-Itacaiúnas, Tapajós-Parima/Ventuari-Tapajós and Rio Negro/Juruena provinces) were accreted to a Siderian-Archean block (e.g. Central Amazon province).

Regional geological maps (e.g. Almeida et al. 2000, Reis et al. 2006, Mendes et al. 2020) and available geochronological data (e.g. Almeida et al. 2000, 2022, Santos et al. 2000, Bizzi et al. 2004, Veras et al. 2018, Carneiro et al. 2017, Mendes et al. 2021) show that Mesoproterozoic to Paleoproterozoic granitoids, orthogneisses and local metavolcano-sedimentary rocks are dominant in southwestern Guyana Shield, NW of Amazon Craton (**Figure 1**). Based on lithostratigraphic and structural data (Bizzi et al. 2004, Reis et al. 2006, 2021), this granitic-gneissic terrain was divided into two tectono-structural domains, named Imeri (east) and Alto Rio Negro (west). Recently, Almeida et al. (2022) subdivided the Rio Negro-Juruena Province into three different domains based on the distribution of basement rocks (**Figure 2**): Northeastern (e.g. Imeri, San Carlos, and Moura terrains), Central (e.g. Içana Terrain) and Southwestern (e.g. Uaupés Terrain). The "Terrain" denomination was adopted here as a descriptive term, used for an area with preponderance of a particular rock (or group of rocks).

These domains show at least three deformational phases (Rodrigues 2016, Carneiro et al. 2017, Veras et al. 2018, Almeida et al. 2022). The D_n structures are poorly preserved, largely obliterated by the D_{n+1} with N69°W/14°NE as a mean strike. The S_n foliation (low-angle dip) was folded by D_{n+1} generating pervasive step-dipping axial plane foliation (S_{n+1}). According to Veras et al. (2018) and Mendes et al. (2020), the apex of regional metamorphism in D_n took place ~1.78 Ga, interpreted as the result of the collision of Cauaburi Arc with the Tapajós-Parima crust (Almeida et al. 2022), responsible for the first crustal anatexis episode in this region (high-grade and partial melting).

The D_{n+1} is the dominant phase, represented mainly by dextral transpressional shear zones with mean foliation directions of N54°W/79°NE generated under amphibolite facies conditions (720°C; 6 kbars), based on the amphibole-plagioclase mineral pair (Carneiro et al. 2017). The metamorphism reached the anatexis, producing abundant migmatites, and S-type granites (and other crustal-derived granites) were generated also in this event (1.54-1.48 Ga; Almeida et al. 2022; unpublished data).

The foliation plane attitudes of the $D_{n+2}$are variable (N35-50°E/90-70°SE to N50°W/65°SW), probably related to new structures (NE-trending) or reactivation of structures formed during the D_{n+1} event (NW-trending). Kinematic indicators such as S-C fabrics, σ-porphyroclasts, asymmetric boudins, and shear bands are consistent with an oblique N-NW-directed compression, with a significant sinistral sense as suggested by Almeida et al. (2022).

In the northern sector of the Rio Negro-Juruena Province (Almeida et al. 2000, 2022, Reis et al. 2006), regional previous works show that this region is composed of a Paleoproterozoic-Mesoproterozoic granitic-gneiss terrane (1.80-1.50 Ga), with some inliers of metasedimentary successions and minor carbonatitic to mafic-ultramafic intrusions (1.30-1.20 Ga). This paper focuses the discussion on the geochemical and geochronological aspects of the A-type to transitional A-I type granites of Tiquié, Marauiá, and Marié-Mirim Suites,

and coeval felsic volcanic rocks, intruded the calc-alkaline basement (1.80-1.76 Ga) in the later stages of the Cauaburi Arc evolution (**Figure 2**). The studied granitoid rocks crop out in the Northeastern (Marauiá and Marié-Mirim Suites) and Southwestern (Tiquié Suite) domains, showing structural-controlled plutonic bodies (Almeida 1997), sometimes with batholithic dimensions. The Machado Volcanics is a coeval event and occurs also in the Southwestern (Tiquié Suite) in association with metasedimentary successions.

3. Northeastern Domain (Imeri Terrain): Marauiá and Marié-Mirim Suites

The granitic-gneissic basement rocks of the Imeri Terrain (Cauaburi Complex) show mainly monzogranitic to granodioritic compositions, represented by four lithofacies, named Tarsira, Santa Isabel, Cumati (e.g. Almeida et al. 2022) and São Jorge (Carneiro et al. 2017), all them with the similar structural and metamorphic patterns (718°C and 5.8 kbars for D_2 event). Contrasting with the other calc-alkaline lithofacies (1.82-1.76 Ga), the São Jorge spessartite-bearing biotite leucogneisses (monzogranite) are SiO_2-rich (>70%), showing peraluminous and alkaline chemistry, similar to A-type granites (Carneiro et al. 2017) but no geochronological-isotopic data are available yet.

Granitoid rocks with A-type chemical affinity are also represented by stocks and batholiths (> 2.800 km²) of the Marauiá (Almeida et al. 2000) and Marié-Mirim (Almeida 1997) suites. These granitoids intrude the granitic-gneissic basement of the Northeastern Domain (Imeri Terrain, Cauaburi Complex), showing dominantly NE-SW (and minor NW-SE) structurally controlled emplacement and elongated shapes (**Figure 2**). Deformation under brittle to brittle-ductile conditions predominates in these granitic bodies, reflecting dynamic recrystallization and fractures/faults. According to Almeida et al. (2000), the Marié-Mirim granite shows potential for cassiterite and Nb, while Marauiá granites show Sn, Nb, and REE (stream sediment), including pegmatite minerals such as topaz, smarskite and ilmenite-rutile, suggesting associated greisenized/albitized rocks.

The granitoids of the Marauiá Suite are pale gray to pale pink, equigranular and medium to coarse-grained, locally porphyritic (subhedral alkali feldspar megacrystals, 2cm in length), with discontinuous and spaced NE-trending foliation. Monzogranites are dominant, with hololeucocratic types and subordinated syenogranites (**Figure 3a**). The main varietal minerals are biotite (<10%), and more rarely hastingsite (<2%), occurring as aggregates with a preferred orientation, defining a unidirectional and anastomosed alignment. The feldspar porphyroclasts are strongly fractured and sometimes replaced

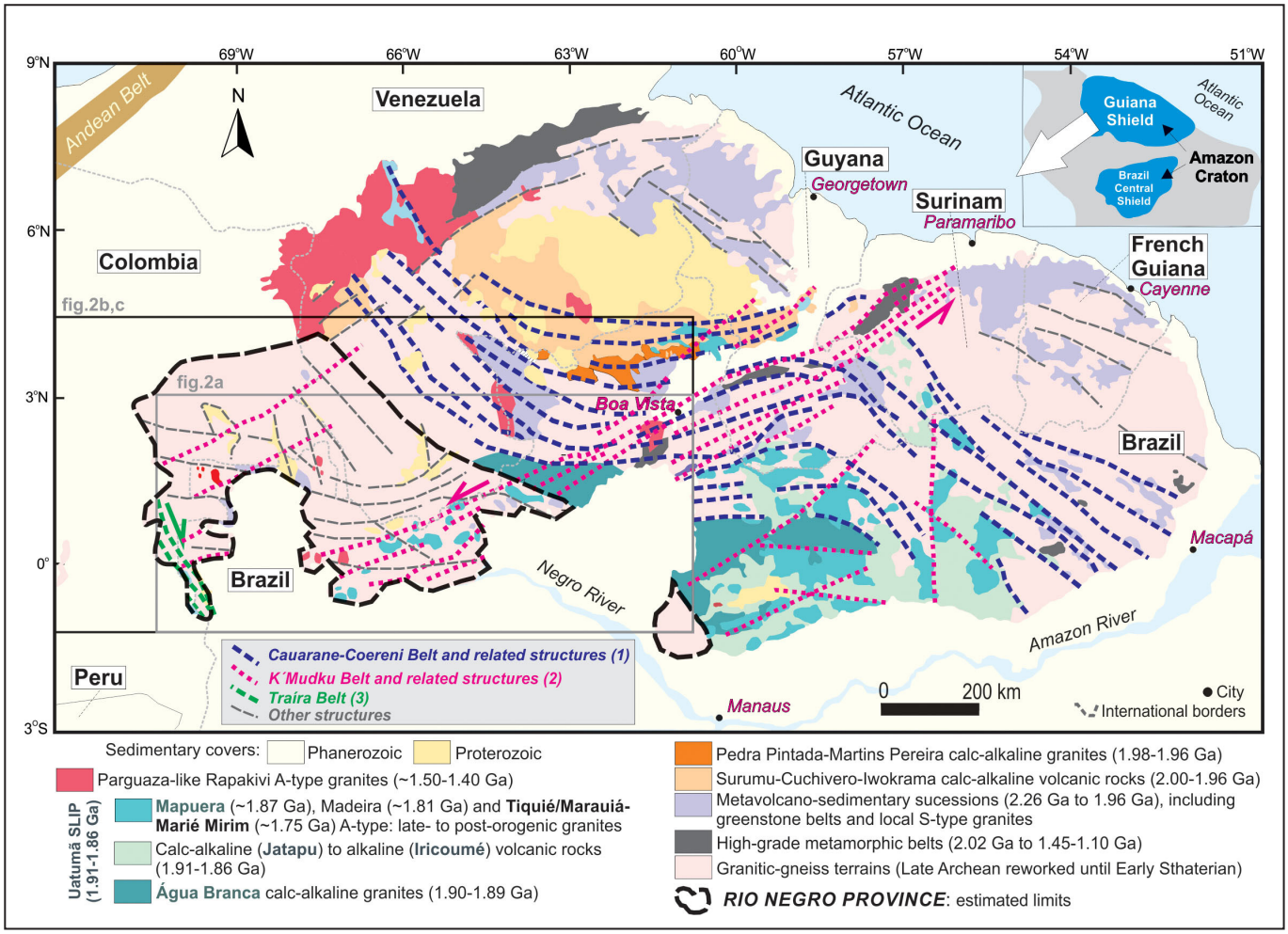

FIGURE 1. Geological sketch map of Guiana Shield (after Gibbs and Barron 1993, modified by Almeida et al. 2022) and location of the study area. For study area details see Figure 2 (gray and black rectangles). Note: (1) Cauarane-Coeroeni Orogenic Belt (CCOB) modified by Fraga et al. (2009); (2) K´Mudku Shear Belt (KSB) modified of Santos et al. (2000); (3) Traíras Shear Belt (TSB) of Almeida et al. (2022).

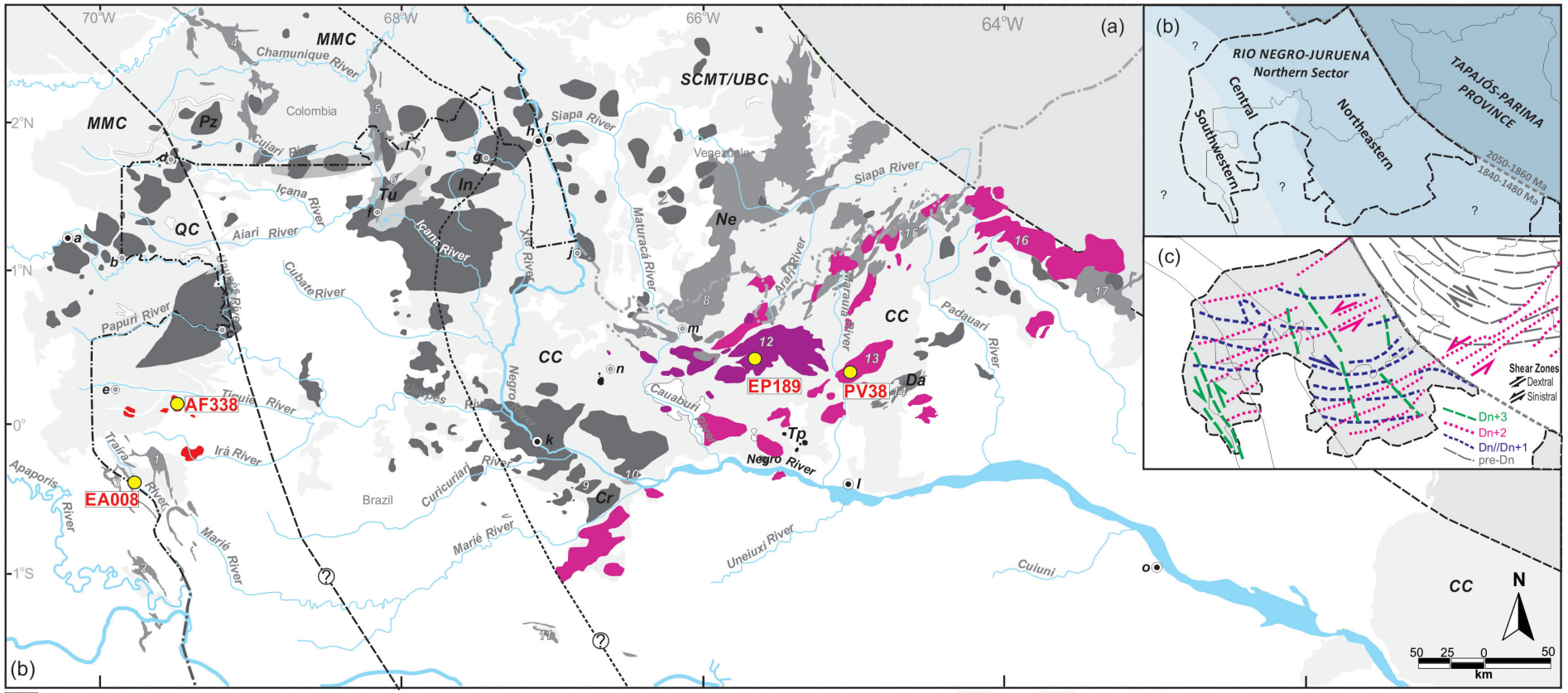

FIGURE 2. (a) Geological sketch map of the NW Amazon Craton modified of Almeida et al. (2000, 2011, 2022), Hackley et al. (2006), Tapias and Meléndez (2015) and Wynn et al. (1993), with emphasis on ~1.75 Ga granites of northern sector of the Rio Negro-Juruena (or Rio Negro) Province and site sampled for geochronological analysis. Simplified (b) tectonic domains and (c) structural framework of the basement rocks.

by sericite, showing undulose extinction and comminution in the borders and along the fractures, locally with subgrains. Quartz ribbons with new grains and subgrains are obliquely elongated, reflecting the last strain increment. Hastingsite occurs as porphyroclasts internally fractured, lenticular, and connected by trails associated with biotite, titanite, and epidote. The observed microtectonic features are compatible with temperature conditions from greenschist to epidote amphibolite facies. The accessory minerals are titanite (<2%), epidote (<1%), allanite (<0,5%), magnetite (<0,5%), apatite (<0,5%) and zircon (<0,5%), with fluorite (<0,5%), chlorite (<0,5%), muscovite/sericite (<3%) and leucoxene (<0,5%) as secondary minerals.

The Marié-Mirim Suite (**Figure 3b**) is characterized by reddish to pale pink syenogranites and alkali-feldspar granites with low mafic minerals content (<1% to 4%), medium- to coarse-grained, equigranular texture and abundant evidence of cataclastic texture. The mineral assemblage is formed by perthitic alkalifeldspar, quartz, plagioclase (albite-oligoclase), biotite, aegirine, riebeckite-arfvedsonite, and muscovite. Accessory minerals include allanite, epidote, opaque minerals, zircon, fluorite, apatite, and titanite. Perthitic alkali-feldspar with spots and ribbons of albite is frequent, while rapaki texture is uncommon. These spots and ribbons show preferred orientation, suggesting fluid transport direction (sodic metasomatism). Graphic intergrowth and abundant cracking filled by quartz-feldspathic material are also observed. Tabular plagioclase shows discrete normal magmatic zoning with cores deeply altered for sericite and epidote, sometimes with cracks, curved twinning lamellae, and twinning slip-along cleavages. Quartz is fine- to medium-grained varying from slight undulose extinction, serrated grains to subgrains generation and abundant cracking, suggesting recrystallization under low-T (< 450°C) and higher strain rates. Biotite is medium-grained, showing apatite, zircon, and fluorite inclusions, in general, associated with allanite, epidote, opaque minerals, and riebeckite-arfvedsonite. Biotite may be replaced by muscovite/sericite and chlorite from the cleavages. Epidote and allanite in magmatic zoning are observed.

Gray to greenish syenite is very rare, showing porphyritic texture, local granoblastic features, and mineral assemblage represented by orthoclase, plagioclase, aegirine, hornblende, titanite, allanite, apatite, epidote and opaque minerals (Melo and Villas Boas 1993).

4. Southwestern Domain (Uaupés Terrain): Tiquié Suite and Machado Formation

The granitoids of the Tiquié Suite (Pinheiro et al. 1976, Lima and Pires 1985) occur as subcircular and small bodies (**Figure 2**), varying from 15 km^2 to exceptionally 1.300 km^2, all of them located in the Southwestern Domain (Uaupés Terrain). The emplacement of these bodies is not structurally controlled, however, some of them are coincidentally positioned next to E-W structures (D_n//D_{n+1}). The basement rocks in this domain are represented by the Querari Complex (1.74-1.70 Ga) and remnants of the Cauaburi Complex (1.81-1.76 Ga), located respectively in the northern and southern areas (e.g. Almeida et al. 2022). The Tiquié granitoids intrude the Cauaburi basement in the southern area, mainly in the Irá River, Castanho, and Onça Creeks (Tiquié river basin). In the type area, Melo and Villas Boas (1993) also describe endogreisens related to the Tiquié magmatism. Lima and Pires (1985) correlate the volcanic rocks (Machado Formation, this study) cropping out in the Traíras River region to the same magmatic event of the Tiquié granitoids. The latter was for many years correlated to the Parguaza event (e.g. Pinheiro et al. 1976), defined in Venezuela (Mendoza 1972), based on whole-rock Rb-Sr conventional analyses (1601 ± 54 Ma and 1583 ± 54 Ma; Pinheiro et al. 1976). Melo and Villas Boas (1993) show that Tiquié granites have geochemical evidence for Sn (stream sediment: 15-70 ppm), Nb and Ti (soil: 1%), and locally pyrite (heavy minerals <1%).

The Tiquié Suite (e.g. Lima and Pires 1985, Almeida 1997) is represented by dark gray to pale pink monzogranites to syenogranites (dominant) with textures varying from equigranular to porphyritic (**Figure 3c,d**), showing fine to coarse-grained matrix and alkalifeldspar megacrystals (1.0-3.0 cm), further hydrotermalized types (**Figure 3e**) cross-cut by quartz-feldspatic veins (**Figure 3f**). The mafic minerals vary from <1% to 8%, occurring as local millimeter-size subcircular mafic aggregates (“mottled” texture). The mineral assemblage is formed by quartz, alkalifeldspar (mainly perthitic), plagioclase, biotite, and hornblende. Accessory minerals are titanite, allanite epidote, apatite, zircon, and opaque minerals (magnetite) whereas the secondary minerals are epidote, fluorite, chlorite, calcite, sericite, and titanite.

The dominant alkalifeldspar is of tabular perthitic type with rare albite rims (rapakivi texture), sometimes with fractures and millimeter-wide quartz veins. The plagioclase (oligoclase-albite) shows discontinuous and oscillatory zoning, sometimes with corroded cores and rims, suggesting instabilities in the magmatic chamber triggered by abrupt P-T variations. The calcic zones are locally transformed into carbonates and fine-grained epidote. Two generations of quartz were observed: 1. fine- to medium-grained and hypidiomorphic crystals, dominant in the matrix and as inclusions; 2. subordinated interstitial, medium-grained and xenomorphic crystals, locally with fractures, undulose extinction and subgrains (low-T dynamic recrystallization). Biotite is medium-grained, hypidiomorphic to xenomorphic, showing apatite, zircon, and fluorite inclusions and secondary replacement by sericite and chlorite. Biotite, opaque minerals, titanite, and epidote occur in mineral association.

Greenish gray felsic volcanics (aphyric) and subvolcanic granites (porphyritic) crop out in the Machado Falls along the Traíras River (**Figure 3g,h**), in the Brazil-Colombia border, grouped in the Machado Formation (this study). In the porphyritic types, plagioclase (lath-shaped/tabular, 5-8 mm) and alkali-feldspar (rounded, 10 mm) are the main phenocrysts, with subordinated “smoked” euhedral quartz (3-5 mm). The matrix is aphanitic to cryptocrystalline, isotropic, and showsstrong secondary alteration for epidote, chlorite, and sericite. These rocks are associated with quartzites, sericite quartzites, and rarely carbonaceous phyllites of the Tunuí Group. The quartzites shows EW/10-35°N compositional banding (So) reworked by structural events as D_n//D_{n+1} (N70°-80°E/70°NW-90°), D_{n+2} (N40°E/40°SW) and D_{n+3} (N60°W/60-70°NE). This last one is responsible for the tectonic framework of the Traíras Shear Belt (younger than 1.30 Ga), producing foliation, shear zones, and folds. A fracture system with N15°W (22°SW to subvertical dips) and N60°E (75°SE dip) strikes is also observed. Milky quartz veins with N80°E trend and vertical dipping are common.

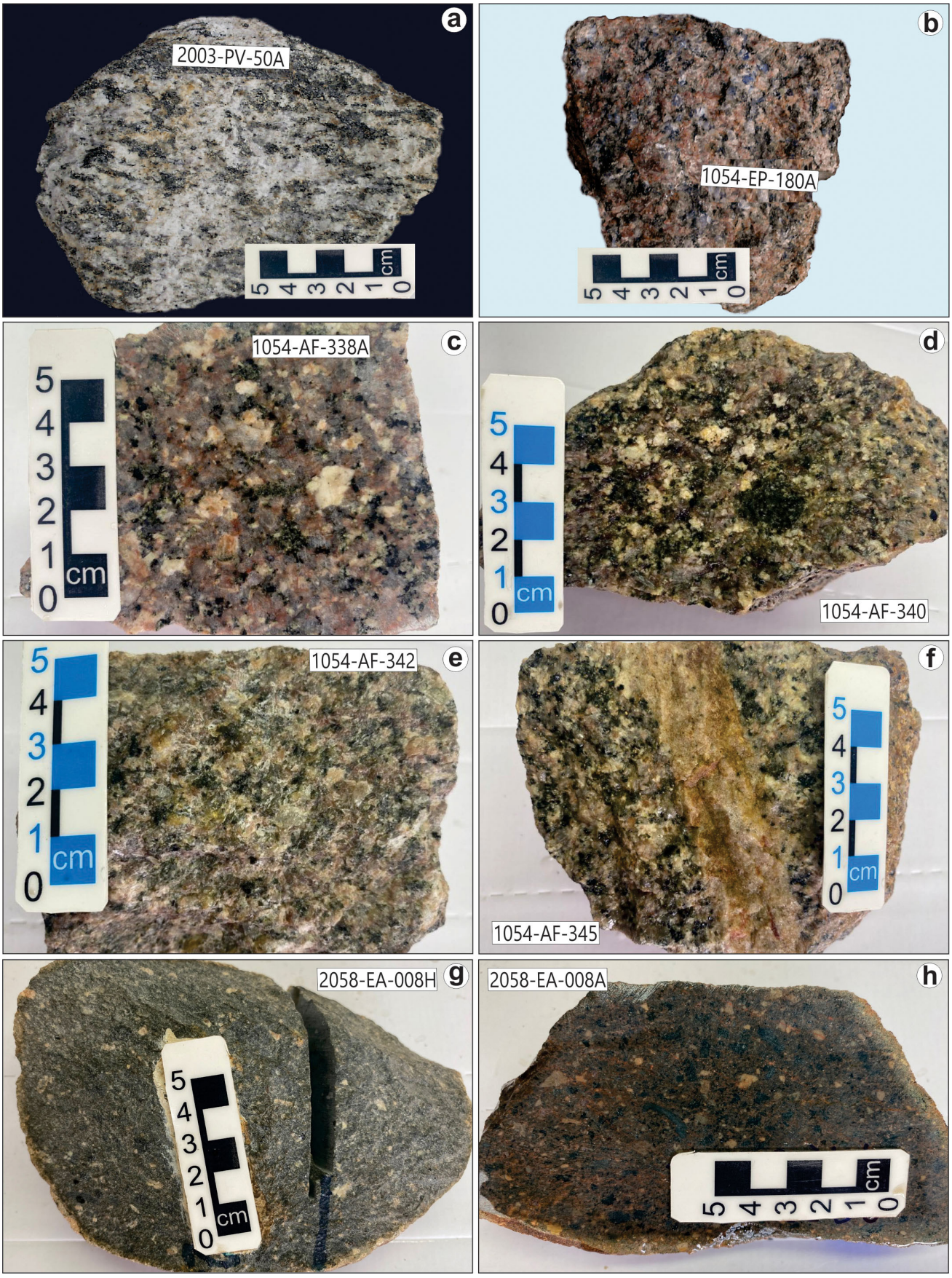

FIGURE 3. (a) Pale gray, equigranular and coarse-grained monzogranites, generally with NE-trending foliaton (Marauiá Suite); (b) Reddish to pale pink, coarse to fine-grained, microperthitic alkalifedspar granites to monzogranites, with blue quartz and cataclastic features (Marié-Mirim Suite); (c) Pale pink porphyritic granites (d) locally with centimeter-long mafic microgranular enclave (Tiquié Suite): (e) Hydrothermalised (epidote/chlorite) granite, (f) sometimes cross-cutted by quartz-feldspathic veins (Tiquié Suite); (g) Rhyodacite (Cachoeira do Machado Formation); (h) Rhyolite porphyry (Cachoeira do Machado Formation).

5. Analytical Procedures

5.1 Whole-rock Geochemistry Analyses

Whole-rock chemical analyses of 27 samples (**Table 1**) were done at the Acme Analytical Laboratories Ltd – AcmeLab (This study), LAMIN/SGB-CPRM (Almeida 1997), and SGS Geosol Laboratories S.A. (Pinheiro et al. 1976, Almeida et al. 2000).

In the AcmeLab the samples were analyzed by inductively coupled plasma-atomic emission spectrometer (ICP-AES) after LiO_2 fusion for all major oxides (SiO_2, TiO_2, Al_2O_3, MnO,

Table 1. Whole-rock chemical compositions of ~1.75 Ga granites of NW Amazon craton. Abbreviations: Aeg. Aegirine; Aln. Allanite; Bt. Biotite; Ep. Epidote; Hs. Hastingsite; Ops. Opaque minerals; Ttn. Titanite. Mineral abbreviations according to Siivola and Schmid (2007).

	Marauiá Suite												
Sample	**AS-50A[4]**	**PV-0[4]**	**PV-53[4]**	**AS-40[4]**	**AS-32[4]**	**JH-20[4]**	**PV-38[1]**	**PV-37[4]**	**AS-41[4]**	**PV-48A[4]**	**JH-21[4]**	**AS-31[4]**	**PV-91[4]**
Clasification	na	na	na	Bt mon-zo-granite (Hs 2%; Ttn 2%)	Bt mon-zo-granite (Hs 1%)	Leu-co-mon-zo-granite	Leu-co-mon-zo-granite (Hs 2%)	Bt ye-no-granite (Ttn 2%)	Leuco-mon-zo-granite (Ep 1%)	Leuco-mon-zo-granite (Hs 1%)	Bt sye-no-granite	Bt mon-zo-granite	Bt sye-no-granite
SiO_2	-	-	-	70.80	72.60	73.30	73.87	73.60	73.90	74.00	74.80	76.30	78.50
TiO_2	-	-	-	0.63	0.21	0.26	0.37	0.21	0.21	0.20	0.10	0.10	0.15
Al_2O_3	-	-	-	13.20	13.20	13.20	12.96	12.30	13.20	13.30	12.30	12.30	11.50
FeO_t	-	-	-	3.62	1.58	2.14	1.84	1.19	1.27	2.00	1.94	0.77	1.18
MnO	-	-	-	0.13	0.06	-	0.05	-	0.05	0.11	-	-	0.90
MgO	-	-	-	0.62	0.17	0.07	0.22	0.40	0.17	0.26	0.11	-	-
CaO	-	-	-	2.10	0.77	0.70	0.90	0.84	1.20	0.18	0.61	0.70	0.39
Na_2O	-	-	-	3.50	3.40	3.50	3.41	4.10	3.20	3.60	3.50	3.20	2.90
K_2O	-	-	-	3.60	6.30	5.60	5.36	6.10	5.80	5.40	5.30	5.10	4.90
P_2O_5	-	-	-	0.31	0.07	0.06	0.05	-	0.11	-	-	0.02	-
LOI	-	-	-	0.90	0.84	0.86	0.50	0.86	0.54	0.16	0.92	0.88	0.21
TOTAL	-	-	-	99.41	99.20	99.69	99.53	99.60	99.65	99.21	99.58	99.37	100.63
Mg Number	-	-	-	23.39	16.09	5.51	17.60	37.40	19.26	18.81	9.18	-	-
Na_2O/K_2O	-	-	-	0.97	0.54	0.63	0.64	0.67	0.55	0.67	0.66	0.63	0.59
A.I.=(K+Na)/Al	-	-	-	0.80	1.11	1.03	1.02	1.24	1.03	1.01	1.07	1.01	1.02
(ppm)													
Ni	-	-	-	-	-	-	1	-	-	-	-	-	-
Co	-	-	-	-	-	-	3	-	-	-	-	-	-
Sc	11	20	14	30	-	-	8	-	25	-	-	-	-
V	11	20	14	30	21	20	10	-	25	20	20	-	20
Cu	-	-	-	-	-	-	2	-	-	-	-	-	-
Pb	6	-	5	5	-	-	7	-	7	-	-	-	-
Zn	-	-	-	-	-	-	50	-	-	-	-	-	-
In	-	-	-	-	-	-	-	-	-	-	-	-	-
Sn	6	-	5	5	-	-	2	-	7	-	-	5	-
W	21.0	-	16.0	28.0	-	-	0.3	-	29.0	-	-	-	-
Mo	-	-	-	-	-	-	0.4	-	-	-	-	-	-
As	1.00	1.00	1.00	0.53	1.10	1.11	0.90	1.08	0.88	1.70	1.16	1.07	1.30
Sb	34.01	-	25.91	45.34	51.82	-	0.10	-	46.96	-	-	43.72	-
Ag	-	-	-	-	-	-	0.1	-	-	-	-	-	-
Au (ppb)	15.4	-	42.2	36.0	31.9	-	1.1	-	39.1	-	-	26.8	-
Rb	310	-	190	220	290	-	175	-	270	-	-	220	-
Cs	-	-	-	-	-	-	1.70	-	-	-	-	-	-
Ba	310	1060	540	730	750	520	468	-	530	345	370	180	100
Sr	100	245	120	250	290	65	77	-	310	45	50	62	20
Tl	-	-	-	-	-	-	0.2	-	-	-	-	-	-
Ga	-	-	-	-	-	-	20	-	-	-	-	-	-
Ta	-	-	-	-	-	-	1.7	-	-	-	-	-	-
Nb	21.0	-	16.0	28.0	32.0	-	24.0	-	29.0	-	-	27.0	-
Hf	-	-	-	-	-	-	11.6	-	-	-	-	-	-
Zr	150	-	410	350	310	-	383	-	380	-	-	260	-
Y	63	-	44	87	28	-	31	-	62	-	-	18	-
Th	19	-	15	46	51	-	19	-	130	-	-	78	-
U	-	-	-	-	-	-	4.4	-	-	-	-	-	-
La	26.79	-	43.70	102.50	68.68	-	62.60	-	149.90	-	-	77.23	-
Ce	56.06	-	198.40	181.80	199.40	-	114.40	-	294.60	-	-	175.40	-
Pr	-	-	-	-	-	-	13.86	-	-	-	-	-	-
Nd	22.69	-	42.81	69.29	45.70	-	49.60	-	74.62	-	-	44.81	-
Sm	4.28	-	8.24	10.73	7.01	-	8.60	-	10.23	-	-	6.22	-
Eu	0.44	-	0.66	1.43	0.70	-	0.58	-	1.46	-	-	0.51	-
Gd	2.81	-	6.53	7.62	4.30	-	5.25	-	7.11	-	-	3.49	-
Tb	-	-	-	-	-	-	0.89	-	-	-	-	-	-
Dy	2.76	-	6.99	8.14	3.84	-	5.38	-	6.48	-	-	3.58	-
Ho	0.59	-	1.45	1.78	0.80	-	1.00	-	1.43	-	-	0.75	-
Er	1.78	-	4.16	5.66	2.30	-	3.02	-	4.51	-	-	2.18	-
Tm	-	-	-	-	-	-	0.49	-	-	-	-	-	-
Yb	1.63	-	4.50	6.09	2.96	-	4.00	-	5.10	-	-	2.39	-
Lu	0.23	-	0.62	0.86	0.41	-	0.53	-	0.75	-	-	0.33	-
TOTAL REE	**120.05**	**-**	**318.05**	**395.90**	**336.10**	**-**	**270.20**	**-**	**556.19**	**-**	**-**	**316.90**	**-**

Table 1 - Continued

	Marauiá Suite												
Sample	**AS-50A[4]**	**PV-0[4]**	**PV-53[4]**	**AS-40[4]**	**AS-32[4]**	**JH-20[4]**	**PV-38[1]**	**PV-37[4]**	**AS-41[4]**	**PV-48A[4]**	**JH-21[4]**	**AS-31[4]**	**PV-91[4]**
Clasification	na	na	na	Bt mon-zo-granite (Hs 2%; Ttn 2%)	Bt mon-zo-granite (Hs 1%)	Leu-co-mon-zo-granite	Leu-co-mon-zo-granite (Hs 2%)	Bt ye-no-granite (Ttn 2%)	Leuco-mon-zo-granite (Ep 1%)	Leuco-mon-zo-granite (Hs 1%)	Bt sye-no-granite	Bt mon-zo-granite	Bt sye-no-granite
Rb/Sr	3.1	-	1.6	0.9	1.0	-	2.3	-	0.9	-	-	3.5	-
Eu(n)/Eu*	0.4	-	0.3	0.5	0.4	-	0.2	-	0.5	-	-	0.3	-
$(La/Yb)_n$	11.1	-	6.5	11.3	15.6	-	10.6	-	19.8	-	-	21.8	-
$(La/Sm)_n$	3.9	-	3.3	6.0	6.2	-	4.6	-	9.2	-	-	7.8	-
$(Gd/Yb)_n$	1.4	-	1.2	1.0	1.2	-	1.1	-	1.1	-	-	1.2	-

References: [1] This paper; [2] Pinheiro et al. (1976); [3] Almeida (1997); [4] Almeida et al. (2000).

	Marié-Mirim Suite							Tiquié Suite						
Sample	**EP-189[1]**	**PT-03[2]**	**PT-36[2]**	**IC-44[2]**	**EP-185[3]**	**EP-186[3]**	**EP-187[3]**	**AF-338[1]**	**AF-339[3]**	**AF-346A[3]**	**AF-340[3]**	**AF-345[3]**	**AF-342[3]**	**AF-343[3]**
Classification	Leuco-syeno-granite	Granite	Aeg granite	Bt granite	Leuco-syeno-granite (Aln-Ops 1%)	Leuco-syeno-granite (Aln-Ops 1%)	Leuco-al-kali-feldspar granite	Monzo-granite	Monzo-granite	Syeno-granite	Syeno-granite	Syeno-granite	Syeno-granite	Syeno-granite
SiO_2	69.92	72.43	73.54	74.12	74.60	74.80	75.10	70.02	71.40	71.40	72.90	74.70	75.10	75.60
TiO_2	0.64	0.39	0.47	0.34	0.22	0.23	0.17	0.46	0.34	0.41	0.25	0.26	0.20	0.16
Al_2O_3	13.82	13.24	13.39	13.09	12.60	12.70	12.60	14.00	13.20	13.40	13.10	12.10	12.00	12.00
FeO_t	2.80	1.94	2.50	2.15	1.17	1.10	0.84	2.65	2.87	2.68	2.25	2.25	1.80	1.81
MnO	0.07	0.10	0.20	0.09	0.05	0.05	0.04	0.07	0.05	0.06	0.04	0.04	0.04	0.03
MgO	0.61	0.41	0.44	0.35	0.09	0.12	0.06	0.75	0.90	0.83	0.70	0.30	0.40	0.30
CaO	2.71	0.68	0.02	1.05	0.29	0.54	0.21	2.27	1.80	1.90	1.20	1.00	0.86	0.83
Na_2O	2.72	2.99	4.12	2.55	4.00	3.80	3.80	3.32	3.50	3.50	3.30	3.10	3.30	3.20
K_2O	5.47	5.83	5.37	6.75	6.00	5.80	6.30	4.89	5.20	4.90	5.60	5.70	5.70	5.40
P_2O_5	0.23	0.04	0.04	0.07	0.05	0.05	0.05	0.17	0.07	0.09	0.05	0.05	0.05	0.05
LOI	0.40	0.35	0.03	0.18	0.18	0.14	0.15	0.80	na	na	na	na	na	na
TOTAL	**99.39**	**98.40**	**100.12**	**100.74**	**99.25**	**99.33**	**99.32**	**99.40**	**99.33**	**99.17**	**99.39**	**99.50**	**99.45**	**99.38**
Mg Number	27.98	23.87	23.88	22.49	12.04	16.24	11.27	33.56	58.54	35.56	63.63	56.12	66.40	64.31
Na_2O/K_2O	0.50	0.51	0.77	0.38	0.67	0.66	0.60	0.68	0.67	0.71	0.59	0.54	0.58	0.59
A.I.=(K+Na)/Al	0.89	1.00	1.06	1.08	1.19	1.13	1.20	0.88	0.99	0.94	1.02	1.10	1.13	1.08
(ppm)														
Ni	2	-	-	-	-	-	-	2	5	5	5	5	5	5
Co	5	-	-	-	5	5	5	5	15	5	5	-	5	5
Sc	11	-	-	-	10	-	-	9	30	20	20	15	10	10
V	32	-	-	-	5	5	5	31	5	20	5	5	50	5
Cu	6	-	-	-	20	100	30	3	30	20	30	50	70	70
Pb	30	-	-	-	10	10	10	15	10	10	10	-	10	10
Zn	66	-	-	-	-	-	-	46	-	-	-	-	-	-
In	-	-	-	-	-	-	-	-	300	200	300	200	150	150
Sn	3	-	-	-	-	-	-	1	-	-	-	-	-	-
W	4.6	-	-	-	-	-	-	0.3	10.0	10.0	10.0	10.0	10.0	15.0
Mo	1.2	-	-	-	-	-	-	0.5	-	-	-	-	-	-
As	2.00	-	-	-	1.54	1.25	1.68	0.70	0.66	0.62	0.86	0.93	1.00	1.00
Sb	0.1	-	-	-	-	-	-	0.1	-	-	-	-	-	-
Ag	0.1	-	-	-	-	-	-	0.1	50.0	70.0	100.0	100.0	200.0	30.0
Au (ppb)	0.5	-	-	-	15.4	20.6	10.3	0.6	-	-	-	-	-	-
Rb	301	-	-	-	448	473	453	189	-	-	-	-	-	-
Cs	8.10	-	-	-	-	-	-	4.10	-	-	-	-	-	-
Ba	564	-	-	-	700	700	1500	1027	-	-	-	-	-	-
Sr	182	-	-	-	-	-	100	244	-	-	-	-	-	-
Tl	0.5	-	-	-	10.0	10.0	10.0	0.2	-	-	-	-	-	-
Ga	19	-	-	-	-	-	-	17	-	-	-	-	-	-
Ta	2.8	-	-	-	-	-	-	1.3	-	-	-	-	-	-
Nb	31.3	-	-	-	-	-	-	16.7	-	-	-	-	-	-
Hf	12.5	-	-	-	-	-	-	8.0	-	-	-	-	-	-
Zr	339	-	-	-	150	200	100	293	-	-	-	-	-	-
Y	76	-	-	-	20	70	20	37	10	10	10	10	10	10
Th	90	-	-	-	-	-	-	28	2	2	3	2	3	2
U	13.8	-	-	-	-	-	-	4.8	-	-	-	-	-	-
La	100.50	-	-	-	70.00	150.00	50.00	64.30	-	-	-	-	-	-

Table 1 - Continued

	Marié-Mirim Suite							Tiquié Suite						
Sample	**EP-189[1]**	**PT-03[2]**	**PT-36[2]**	**IC-44[2]**	**EP-185[3]**	**EP-186[3]**	**EP-187[3]**	**AF-338[1]**	**AF-339[3]**	**AF-346A[3]**	**AF-340[3]**	**AF-345[3]**	**AF-342[3]**	**AF-343[3]**
Classification	Leuco-syeno-granite	Granite	Aeg granite	Bt granite	Leuco-syeno-granite (Aln-Ops 1%)	Leuco-syeno-granite (Aln-Ops 1%)	Leuco-al-kali-feldspar granite	Monzo-granite	Monzo-granite	Syeno-granite	Syeno-granite	Syeno-granite	Syeno-granite	Syeno-granite
Ce	182.70	-	-	-	-	-	-	108.50	-	-	-	-	-	-
Pr	23.63	-	-	-	-	-	-	12.73	-	-	-	-	-	-
Nd	83.70	-	-	-	-	-	-	45.40	-	-	-	-	-	-
Sm	14.40	-	-	-	-	-	-	7.20	-	-	-	-	-	-
Eu	2.21	-	-	-	-	-	-	1.39	-	-	-	-	-	-
Gd	10.49	-	-	-	-	-	-	5.56	-	-	-	-	-	-
Tb	1.87	-	-	-	-	-	-	1.00	-	-	-	-	-	-
Dy	11.64	-	-	-	10.00	10.00	10.00	5.59	-	-	-	-	-	-
Ho	2.33	-	-	-	-	-	-	1.18	-	-		-	-	-
Er	6.71	-	-	-	-	-	-	3.33	-	-	-	-	-	-
Tm	1.12	-	-	-	-	-	-	0.45	-	-	-	-	-	-
Yb	7.91	-	-	-	-	-	-	3.86	-	-	-	-	-	-
Lu	1.21	-	-	-	-	-	-	0.55	-	-	-	-	-	-
TOTAL REE	**450.42**	**-**	**-**	**-**	**-**	**-**	**-**	**261.04**	**-**	**-**	**-**	**-**	**-**	**-**
Rb/Sr	1.7	-	-	-	-	-	4.53	0.8	-	-	-	-	-	-
Eu(n)/Eu*	0.5	-	-	-	-	-	-	0.6	-	-	-	-	-	-
$(La/Yb)_n$	8.6	-	-	-	-	-	-	11.2	-	-	-	-	-	-
$(La/Sm)_n$	4.4	-	-	-	-	-	-	5.6	-	-	-	-	-	-
$(Gd/Yb)_n$	1.1	-	-	-	-	-	-	1.2	-	-	-	-	-	-

References: [1]This paper; [2]Pinheiro et al. (1976); [3]Almeida (1997); [4]Almeida et al. (2000). Abbreviations: Aeg. Aegirine; Aln. Allanite; Bt. Biotite; Ep. Epidote; Hs. Hastingsite; Ops. Opaque Minerals; Ttn. Titanite.

MgO, CaO, K_2O, Na_2O, P_2O_5) and LOI, and inductively coupled plasma-mass spectrometer (ICP-MS) for trace elements, with rare-earth and incompatible elements determined from a $LiBO_2$ fusion. Precious and base metals were determined from an aqua regia digestion. In the LAMIN/SGB-CPRM only major elements and Rb were analyzed by X-ray fluorescence from glass beads. In the SGS Geosol, all major and trace elements were analyzed by an inductively coupled plasma-atomic emission spectrometer (ICP-OES/ICP-MS) with determination by multi-acid digestion.

5.2 Single zircon Pb-evaporation

The single-zircon dating by Pb-evaporation was performed at the Isotope Geology Laboratory (Pará-Iso), Federal University of Pará (UFPA, Brazil), with all isotope analyses carried out on a Finnigan MAT 262 mass spectrometer in dynamic mode, using the ion counting detector. The Pb-evaporation technique used is the same as established by Kober (1986, 1987). After the mechanical separation of zircon crystals, the selected grains were tied in Re-"evaporation"-filament and introduced in the mass spectrometer. The Pb was normally extracted from the crystals by heating in three evaporation steps at temperatures of 1450°C, 1500°C, and 1550°C. The evaporated Pb was loaded on an "ionization" filament, which was heated for the isotope analyses. Usually, the average $^{207}Pb/^{206}Pb$ ratio obtained in the highest temperature step was taken for the age calculation, but the other steps were also considered when similar to the mean age. Outliers were eliminated using Dixon's test. The $^{207}Pb/^{206}Pb$ ratios were corrected for a mass discrimination factor of 0.12% ± 0.03 per a.m.u, and results with $^{204}Pb/^{206}Pb$ ratios higher than 0.0004 were normally discarded. The ages were calculated with 2 sigma errors and common Pb correction was done using appropriate age values derived from the two-stage model of Stacey and Kramers (1975). The obtained data were processed in the shareware Zircon program, DOS system version.

The Pb-evaporation single zircon method yields apparent $^{207}Pb/^{206}Pb$ ages and the degree of concordance of the analytical points is not possible to assess. Furthermore, zircon grains exhibiting a complex history often yield mixed ages with no geological meaning (Dougherty-Page and Bartlett 1999). With these uncertainties in mind, the age obtained for a single grain is considered as a minimum age; however, several studies (Kober 1986, Ansdell and Kyser 1991, Gaudette et al. 1998, Söderlund 1996) show that if a set of magmatic grains from the same sample yields similar ages, it strongly suggests they indicate the time of magmatic crystallization.

6. Results

6.1 Whole-Rock Multielemental Geochemistry

The petrographic studies of the analyzed samples show monzogranitic to alkali-feldspar granitic compositions. Tiquié, Marié-Mirim and Marauiá suites has syenogranites, leucosyenogranites and monzogranites as dominant compositions, respectively. In the chemical classification diagrams, this pattern is confirmed, as in the TAS diagram (**Figure 4a**; Le Maitre 1976), where all samples occur in the "subalkaline granites" field. Contrasting with petrographic analyses, the R1-R2 multicationic diagram (**Figure 4b**; De la Roche et al. 1980), demonstrates that Tiquié, Marié-Mirim, and Marauiá Suites show dominant monzogranites, alkali-feldspar granites, and syenogranites compositions, respectively.

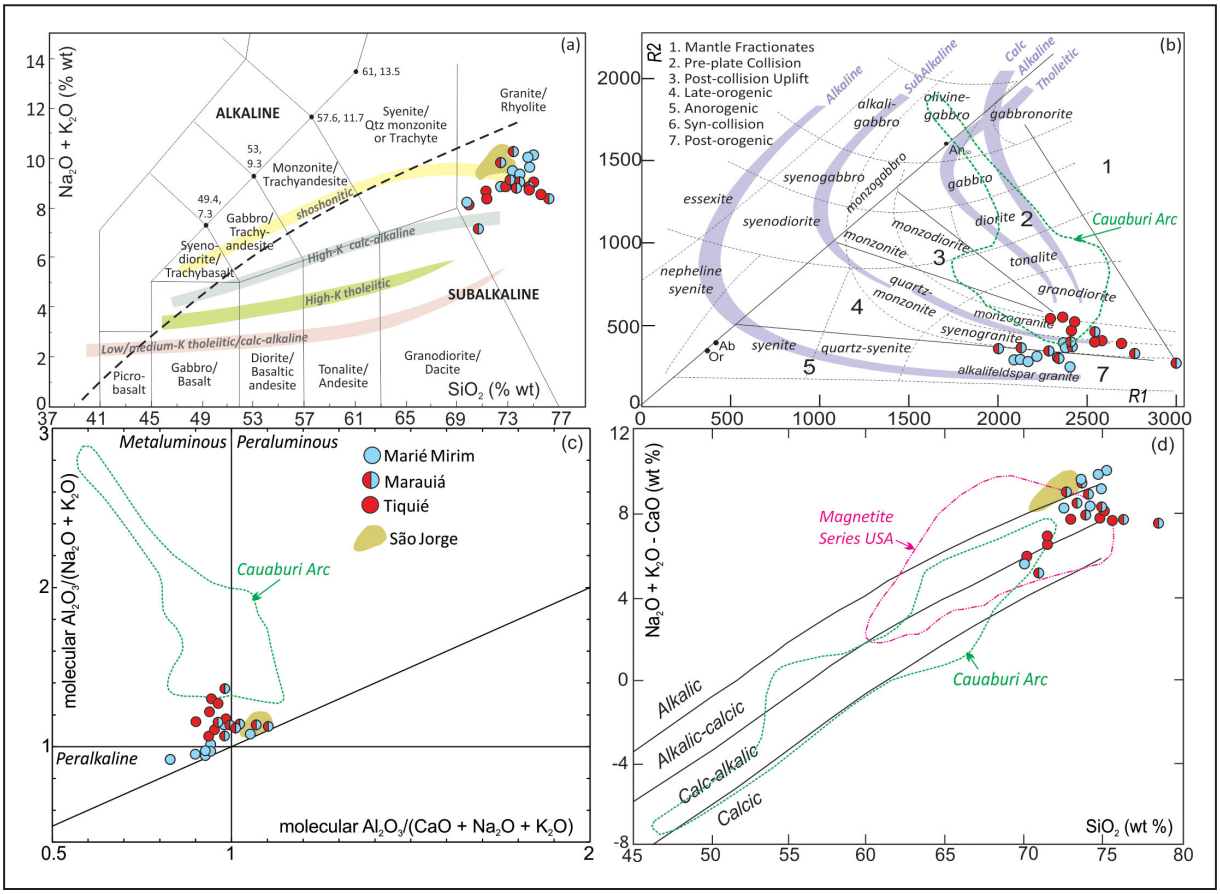

FIGURE 4. Classification diagrams showing granitoid rocks of the Marié-Mirim, Marauiá and Tiquié suites: (a) TAS diagram adapted from Le Maitre (1976) with alkalinity index of Irvine and Baragar (1971); (b) R1 vs. R2 multicationic diagram (De la Roche et al. 1980, Batchelor and Bowden 1985); (c) Shand index in the molar A/NK x A/CNK diagram; and (d) Na_2O+K_2O-CaO x SiO_2 diagram with fields of Frost et al. (2001). The Cauaburi Arc (calc-alkaline magmatism) and São Jorge leucogneisses compositional fields were obtained from Almeida et al. (2022) and Carneiro et al. (2017), respectively.

The Tiquié Suite rocks are metaluminous (**Figure 4c**; *cf.* Shand Index) and alkalic-calcic (**Figure 4d;** *cf.* Frost et al. 2001), SiO_2-rich (70.0-75.6%), transitional among ferroan and magnesian (**Figure 5a**; *cf.* Frost et al. 2001), plotting in the A- and I-type granite fields. These granites are also plotted in the calc-alkaline to metaluminous A-type fields in the Log [CaO/(Na_2O+K_2O)] x SiO_2 diagram (**Figure 5b**). The A-type signature in the Tiquié Suite is more evident in the CaO/(FeO_t+MgO+TiO_2) x CaO+Al_2O_3 (**Figure 5c**; *cf.* Dall'Agnol and Oliveira 2007) and CaO/(FeO_t+MgO+TiO_2) x Al_2O_3 (**Figure 5d**; *cf.* Dall'Agnol and Oliveira 2007) diagrams. Tiquié Suite rocks present low FeO_t/(FeO_t+MgO) ratios, including higher #MgO (33-66), comparable locally to the calc-alkaline granitoid rocks, suggesting probable rich-Mg sources. Other discriminant diagrams, such as Ce/Nb x Y/Nb and Zr x Al/Ga*10000 (**Figures 5e,f**; *cf.* Eby 1992), indicate for Tiquié Suite A-type signatures with higher Y/Nb ratio and lowest Ce/Nb and Al/Ga*10000 ratios if compared with the Marauiá and Marié-Mirim granitoids.

The Marauiá Suite is metaluminous to peraluminous (**Figure 4c**; Shand Index) and alkalic-calcic to calc-alkalic (**Figure 4d;** *cf.* Frost et al. 2001), SiO_2-rich (70.8-78.5%), ferroan (**Figure 5a**; *cf.* Frost et al. 2001), with low #MgO (9-37), plotting in the A-type granite fields. The samples are plotted in the metaluminous A-type fields in the Log [CaO/(Na_2O+K_2O)] x SiO_2 diagram (**Figure 5b**). This A-type signature persists in the CaO/(FeO_t+MgO+TiO_2) x CaO+Al_2O_3 and CaO/(FeO_t+MgO+TiO_2) x Al_2O_3 (**Figure 5c,d**; *cf.* Dall'Agnol and Oliveira 2007) diagrams. In the discriminant diagrams using trace elements, as Ce/Nb x Y/Nb and Zr x Al/Ga*10000 (**Figures 5e,f**; *cf.* Eby 1992), the Marauiá Suite shows A-type signatures with wide variation in the Y/Nb and Ce/Nb ratios and high Zr and Al/Ga*10000 ratios if compared with the Marié-Mirim and Marié-Mirim granitoids.

The Marié-Mirim Suite lithotypes are peralkaline to peraluminous (**Figure 4c**; Shand Index) and alkalic to alkalic-calcic (**Figure 4d;** *cf.* Frost et al. 2001), SiO_2-rich (69.9-75.1%), ferroan to slightly magnesian (**Figure 5a**; Frost et al. 2001) with low #MgO (11-28), plotting in the A-type granite fields. In the Log [CaO/(Na_2O+K_2O)] x SiO_2 diagram this Suite plots partially in the metaluminous A-type granite field, showing very low Log [CaO/(Na_2O+K_2O)] ratios (**Figure 5b**). The A-type pattern is observed in all other diagrams, such as CaO/(FeO_t+MgO+TiO_2) x CaO+Al_2O_3 and CaO/(FeO_t+MgO+TiO_2) x Al_2O_3 (**Figure 5c,d**;*cf.* Dall'Agnol and Oliveira 2007) and Ce/Nb x Y/Nb and Zr x Al/Ga*10000 (**Figures 5e,f**; *cf.* Eby 1992).

In a general sense, the São Jorge leucogneisses are peraluminous, alkalic (**Figure 4c,d**), ferroan, and transitional A1 to A2 type granites (**Figure 5a,e**), showing similarities with more fractionated types of the Marauiá and Marié-Mirim suites. However, these leucogneisses are more enriched in Al_2O_3 (14-16%), presenting lower Ga/Al (**Figure 5f**) and higher

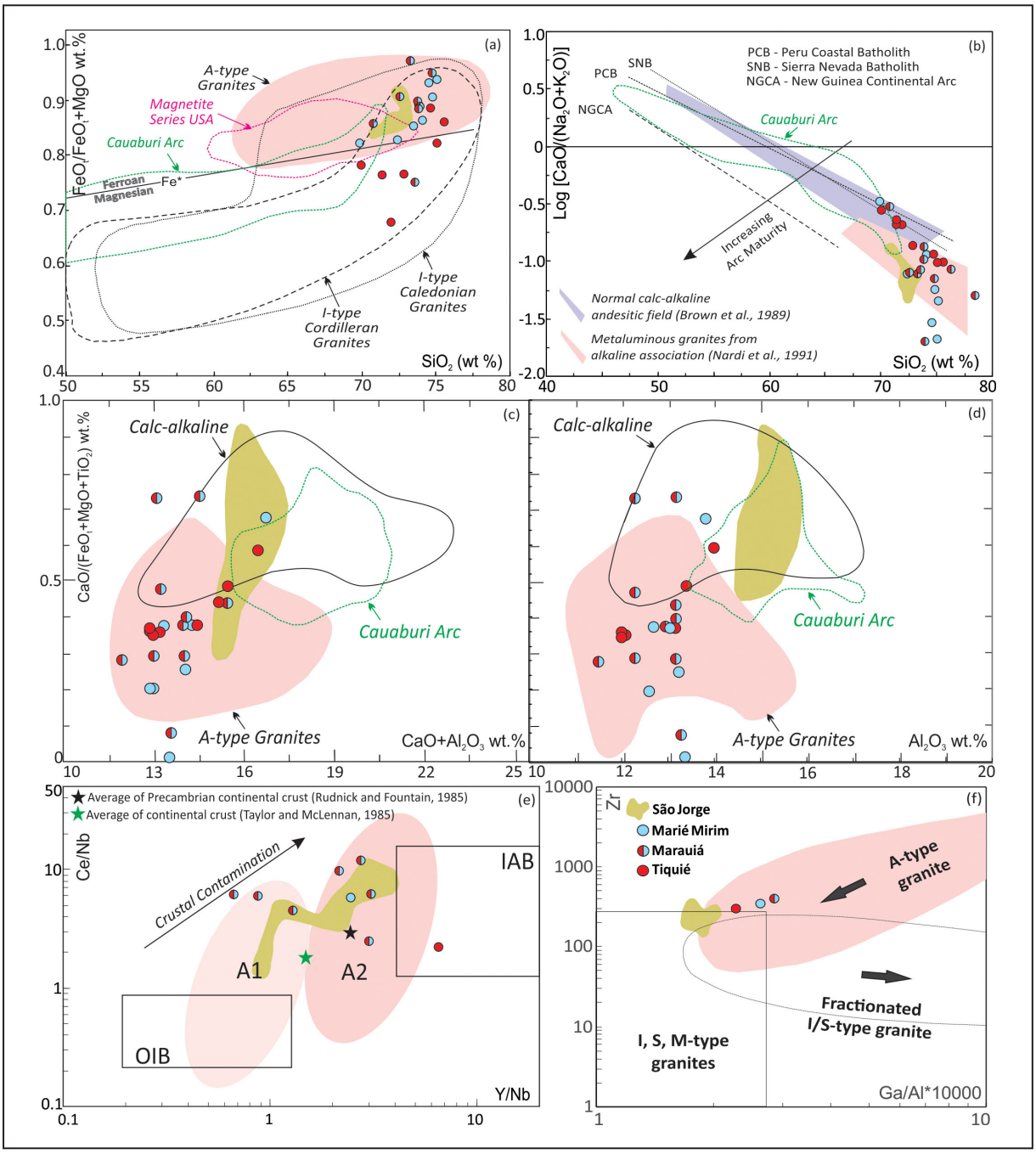

FIGURE 5. Discriminant diagrams showing A-type chemistry for the granitoid rocks of the Marié-Mirim, Marauiá and Tiquié Suites: (a) $FeO_t/(FeO_t+MgO)$ x SiO_2 (*cf.* Frost et al. 2001; Magnetite Series USA: *cf.* Whalen et al. 1987); (b) Log $[CaO/(Na_2O+K_2O)]$ x SiO_2 (*cf.* Brown et al. 1984, Nardi 1991); (c) $CaO/(FeOt+MgO+TiO_2)$ x $CaO+Al_2O_3$ and (d) x Al_2O_3 (*cf.* Dall'Agnol and Oliveira 2007); (e) Ce/Nb x Y/Nb and (f) Zr x Ga/Al * 10000 (*cf.* Eby 1992; A-type and fractionated S/I-type fields: *cf.* FuYuan et al. 2017). The Cauaburi Arc (calc-alkaline magmatism) and São Jorge leucogneisses compositional fields were obtained from Almeida et al. (2022) and Carneiro et al. (2017), respectively.

$CaO/(MgO+FeO+TiO_2)$ ratios, plotting in the calc-alkaline fields, such as the Cauaburi Complex rocks (**Figure 5c,d**).

Two new methods for magma thermometry (Daneshvar et al. 2022), which consider HFSE behavior, suggest high-temperature crystallization to these granitic magmas (Marié-Mirim 1085°C, Tiquié 1150°C and Marauiá 1205°C). Both equations are applicable for temperatures from 750°C to 1400°C and expressed in Kelvin. The first them use an equation specially formulated to metaluminous to peraluminous rocks (Tiquié and Marauiá Suites) with SiO_2> 63 wt.% and M < 2 [(Na + K + 2Ca)/(Al×Si)] (cation ratio): **T(K) = −15,993/(lnCZr + lnCHf – 21.668**; where CZr and CHf are respectively the bulk-rock Zr and Hf contents (ppm) in whole rocks. The second equation is more suitable for peralkaline to alkaline rocks (Marié-Mirim Suite) with M > 2 and a wide range of SiO_2:**T(K) = −20,914/(ln(CHf + CY + CCe) + (ln(CZr/TiO2) – 31.153**; where CHf, CY, and CCe, and CZr are respectively the bulk-rock Hf, Y, Ce, and Zr contents (ppm).

In the Harker diagrams, the analyzed samples show SiO_2negative correlations for TiO_2, Al_2O_3, MgO, CaO, FeO_t, P_2O_5 (**Figure 6**) and dispersion for Na_2O and K_2O, suggesting fractionation of Fe-Ti oxides, biotite, amphibole, plagioclase, and apatite. Marié-Mirim Suite shows higher TiO_2, Al_2O_3, and lowest CaO, MgO, and FeO_t if compared with Tiquié Suite for the same SiO_2 intervals. Overall, the Marauiá Suite has high P_2O_5 and low FeO_t, TiO_2, and MgO contents. The São Jorge leucogneisses do not define the same trend with the studied granites, showing low TiO_2, MgO, P_2O_5, and higher Al_2O_3, this last one is commented above.

In the tectonic discriminant diagrams, the Marauiá, Tiquié, and Marié-Mirim suites plot on the post-collisional granites field (**Figure 7a**; *cf.* Pearce et al. 1984, *cf.* Pearce 1996), near to the boundaries of syncollisional (Marié-Mirim, high Rb), volcanic-arc (Tiquié, low Nb+Y) and within-plate (Marauiá, high Nb+Y) compositions. All samples also plot in the collisional calc-alkaline to alkaline and A2-type fields (**Figure 7b;** *cf.* Thieblèmont and Tégyey 1994). The São Jorge leucogneisses present the same chemical pattern, plotting also in the within-plate and collisional calc-alkaline alkaline and A2-type fields.

In the primitive mantle-normalized spidergram pattern, these granites are concordant with (**Figure 8a**) those of the oxidized A-type Jamon Granite of the Carajás region (Dall'Agnol and Oliveira 2007) and other averages of classical A-types from LFB (Gabbo, Mumbula; White and Chappell 1983) and SW of USA (Anderson and Bender 1989). Locally, the Marié-Mirim and Marauiá granites show lower Ba, P, and Y and higher Th and U. The REE chondrite-normalized patterns of Marauiá, Tiquié, and Marié-Mirim suites are similar **(Figure 8a)**, showing small to moderate negative Eu anomaly (Eu_n/Eu^*: 0.25-0.65), moderate REE fractionation [$(La/Yb)_n$: 1.9-2.9] and REE total (120 to 556 ppm). The compositional envelope of São Jorge leucogneisses for REE and trace elements are coincident with the studied granites.

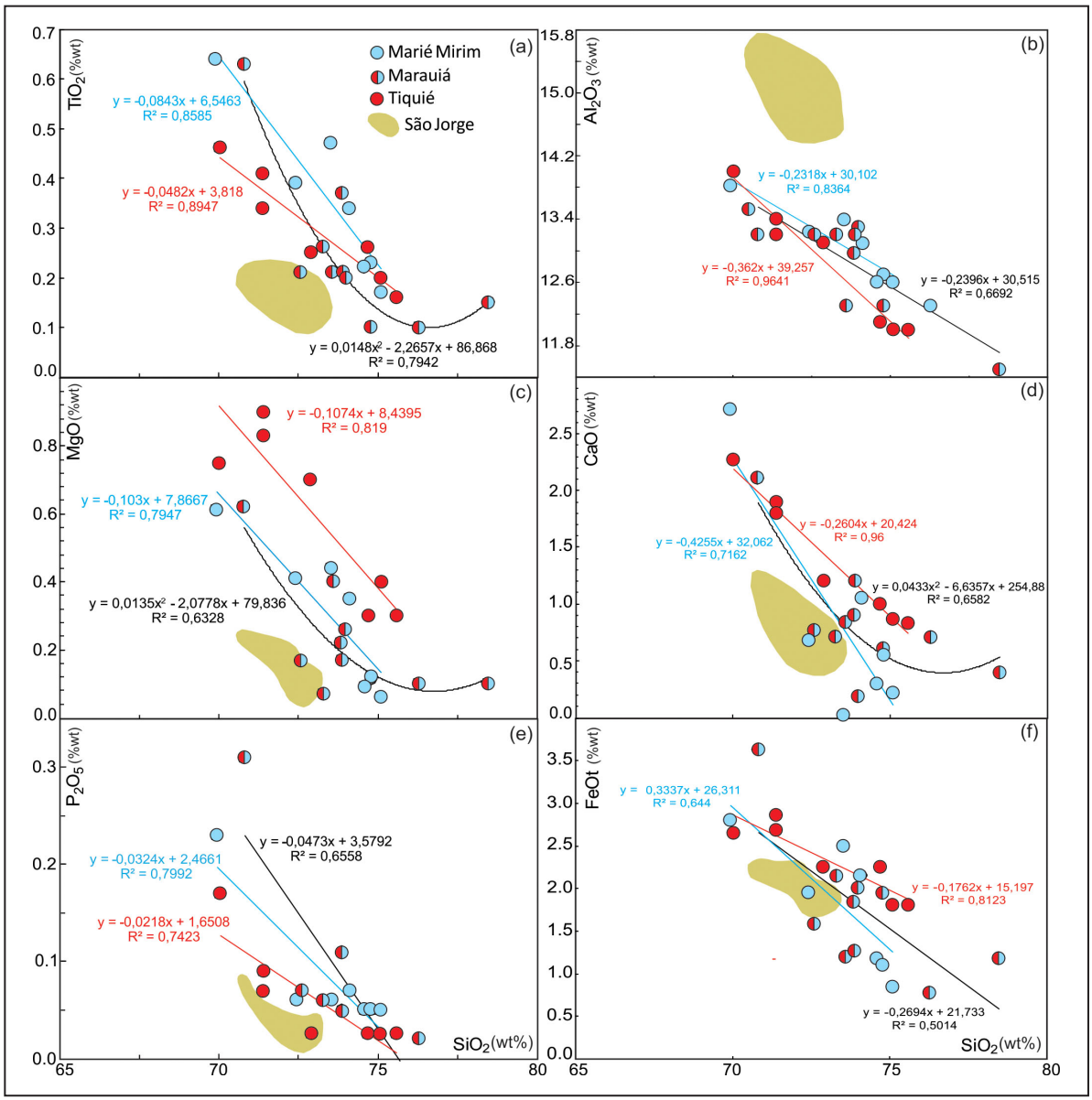

FIGURE 6. (a-f) Selected Harker variation diagrams for samples of ~1.75 Ga granites (Marauiá, Marié-Mirim and Tiquié Suites). For references see Table 1. The São Jorge leucogneisses composition field was obtained from Carneiro et al. (2017).

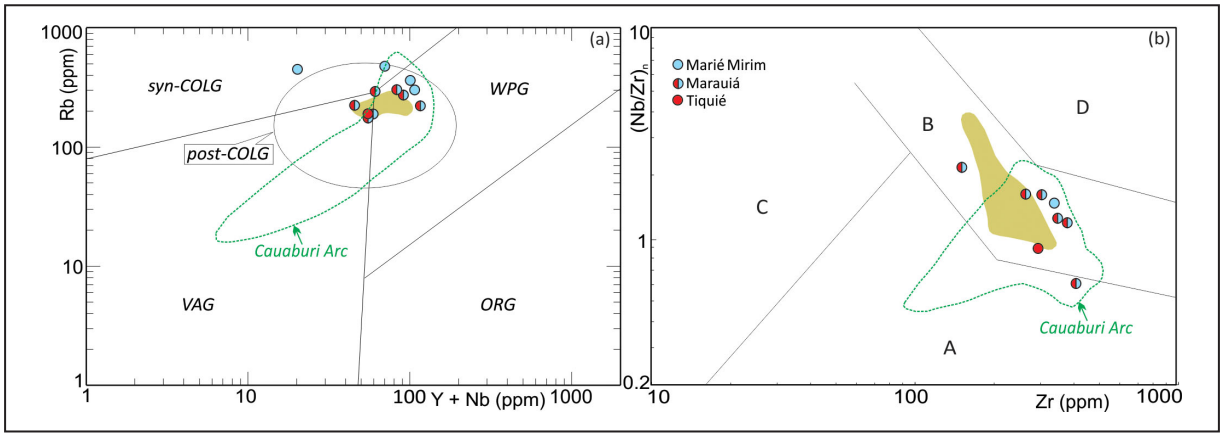

FIGURE 7. Classification and tectonic discriminant diagrams showing granitoid rocks of the Marié-Mirim, Marauiá and Tiquié suites: (a) Rb vs. (Y+Nb) diagram with VAG (Volcanic Arc Granites), ORG (Ocean Ridge Granites), syn-COLG (Syn-collisional Granites), WPG (Within-Plate Granites) fields (*cf.* Pearce et al. 1984) and post-COLG (post-collisional granites; *cf.* Pearce 1996); (b) geotectonic classification of granitoid rocks using $(Nb/Zr)_n$ vs. Zr diagram (*cf.* Thieblèmont and Tégyey 1994). Normalization values (Nb: 0.6175; Zr: 9.714) were taken from Hoffman (1988). Tectonic fields: A. Subduction magmatic rocks; B. Collisional calc-alkaline, alkaline, and A2-type rocks; C. Collisional hyperaluminous rocks; D. Intraplate alkaline rocks and A1-type rocks. The Cauaburi Arc (calc-alkaline magmatism) and São Jorge leucogneisses compositional fields were obtained from Almeida et al. (2022) and Carneiro et al. (2017), respectively.

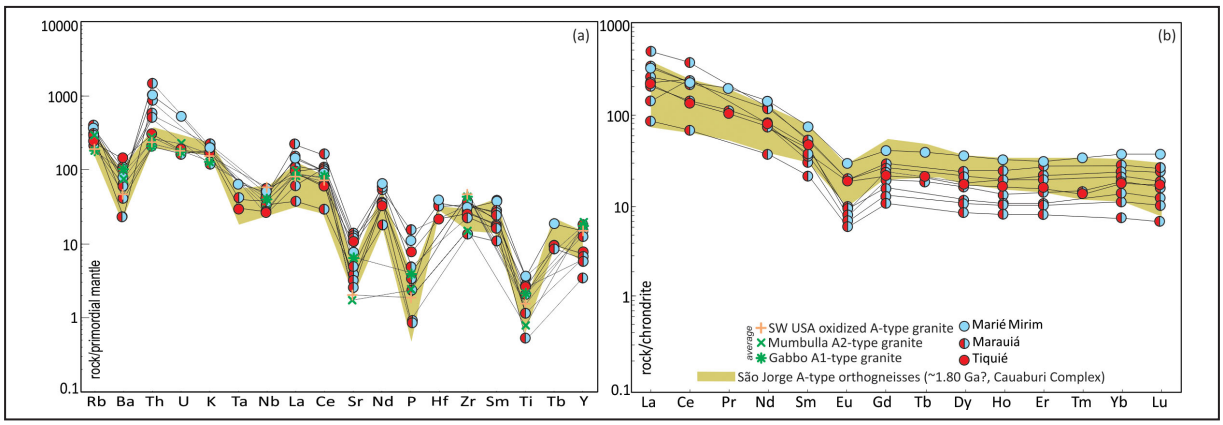

FIGURE 8. (a) Chondrite-normalized REE (Boynton 1984) and (b) primitive mantle-normalized (Wood et al. 1979) multielemental diagrams for the studied granites (Tiquié, Marauiá and Marié-Mirim Suites). The REE envelope of oxidized A-type Jamon Granite (SE Carajás, Pará; Dall'Agnol and Oliveira 2007) is plotted for comparison, including the average composition of Mumbulla, Gabbo (White and Chappell 1983) and SW USA (Anderson and Bender 1989) A-type granites. The São Jorge leucogneisses composition field was obtained from Carneiro et al. (2017).

6.2 Zircon Geochronology: Pb-Evaporation

Four samples from the type area of the Marauiá, Marié-Mirim, Tiquié, and Cachoeira do Machado magmatism were selected for analyses in the single-zircon Pb-evaporation technique. For the petrography summary and geographic coordinates see **Table 2**.

6.2.1 Northeastern Domain (Imeri Terrain)

Leuco-syenogranite (EP-189 sample; Marié-Mirim Suite)

The EP-189 sample shows colorless to pale brown crystals, transparent and bipyramidal, with prismatic habit (length/width ratios 2:1 to 2.5:1) and ~200 µm in length. They exhibit well-defined faces and local slightly rounded vertices. Mineral inclusions (e.g. apatite, Fe-Ti oxides), fluid inclusions, and cracks are observed. A total of three crystals were analyzed by zircon Pb-evaporation yielding a mean $^{207}Pb/^{206}Pb$ age of 1756 ± 12 Ma (MSWD: 1.5; **Figure 9a**) from 64 isotopic ratios (**Table 3**) and individual ages vary from 1763 Ma to 1748 Ma. This result is interpreted as the crystallization age of the Marié-Mirim magmatism. Five more clear and free inclusions crystals yielded a $^{207}Pb/^{206}Pb$ age of 1805 ± 8 Ma (**Figure 9a**) from 120 isotopic ratios (**Table 3**) and individual ages vary from 1814 Ma to 1797 Ma, interpreted as protolith age of the Cauaburi basement.

Leucomonzogranite with hastingsite (PV-38 sample; Marauiá Suite)

The PV-38 sample shows a zircon population with wide variation in length (100-440 µm), colorless to pale yellow, transparent and bipyramidal, with prismatic habit (length/width

Table 2. Petrography summary and geographic coordinates of analyzed samples by the single-zircon Pb-evaporation technique.
Note: The number of grain analyses used to calculate the age is in parentheses.

Sample code	Stratigraphic unit	Geog. Coord.	Sample description	Single Zircon Pb-evaporation				WR Sm-Nd	
				Crystallization age (Ma)	*Inherited age (Ma)*	*Pb-loss or meta-morphic age (Ma)*	*USD*	*TDM age (Ga)*	*eNd(t)*
EP-189	Marié Mirim Granite, type-area (Marié Mirim Suite)	00° 29' 04" N 66° 13' 23" W	Leuco-syenogranite with equigranular and coarse-grained texture, reddish to pale pink colors. Cataclastic features are common. Accessory minerals: epidote-allanite, magnetite, apatite and zircon. Locally with riebeckite-arfvedsonite.	1756 ± 12 (3zi)	1805 ± 8 (5zi)	-	1.5	1.91	+2.27
PV-38	Marauiá Granite, type-area (Marauiá Suite)	00° 22' 12" N 65° 00' 36" W	Leuco-monzogranite with hastingsite showing pale pink to whitish and equigranular, coarse to medium grained, locally with protomylonitic/mylonitic textures. Accessory minerals: opaque minerals, allanite, titanite, apatite, titanite and zircon.	1746 ± 6 (1zi)	1781 ± 7 (2zi)	1651 ± 7 (1zi) 1714 ± 5 (2zi)	2.1 1.9 2.6	2.01	+0.92
AF-338	Tiquié Granite, type-area (Tiquié Suite)	00° 06' 37" N 69° 29' 24" W	Leuco-syenogranite with equigranular and coarse-grained texture, reddish to pale pink colors. Cataclastic features are common. Accessory minerals: epidote-allanite, magnetite, apatite and zircon. Locally with riebeckite-arfvedsonite.	1747 ± 6 (7zi)	2032 ± 2 (1zi)	-	2.9	1.95	+1.76
EA-08	Cachoeira do Machado Volcanic, type-area (Cachoeira do Machado Formation)	00° 22' 50" S 69° 48' 55" W	Rhyodacite with quartz and feldspar phenocrysts and aphanitic to cryptocrystalline groundmass, locally with hydrothermal alteration (e.g. chlorite)	1751 ± 2 (6zi)	-	-	1.8	-	-

ratios 2.5:1 to 3:1), well-defined to slightly corroded faces and local rounded vertices. Mineral inclusions (e.g. apatite, Fe-Ti oxides), fluid inclusions, and cracks are common. Only one crystal yielded a mean $^{207}Pb/^{206}Pb$ age of 1746 ± 6 Ma (MSWD: 2.1; **Figure 9b**) from 58 isotopic ratios (**Table 3**), interpreted as the crystallization age of the Marié-Mirim magmatism. Two crystals yielded a $^{207}Pb/^{206}Pb$ age of 1781 ± 7 Ma (**Figure 9b**) from 46 isotopic ratios (**Table 3**) and individual ages vary from 1788 Ma to 1778 Ma, interpreted also as protolith age of the Cauaburi basement. Three other crystals show 1714 ± 5 Ma and 1651 ± 7 Ma mean $^{207}Pb/^{206}Pb$ ages (Figure 10b), probably related to Pb-loss, with no geological meaningless, however, a metamorphic origin or a younger magmatic event should not be ruled out. Thus, due to the populational complexity of zircons, this sample must be analyzed in the future using high-resolution methods.

6.2.2 Southwestern Domain (Uaupés Terrain)

Biotite monzogranite (AF-338 sample; Tiquié Suite)

The AF-338 sample shows a zircon population with 350-230 **µm** in length, colorless to pale yellow, transparent, and bipyramidal, with prismatic habit (length/width ratios 2:1 to 3:1), well-defined faces, and rarely rounded vertices. Mineral inclusions (e.g. apatite, Fe-Ti oxides), fluid inclusions, and cracks are observed. A mean $^{207}Pb/^{206}Pb$ age of 1747 ± 6 Ma (MSWD: 2.9; **Figure 9c**), obtained from seven crystals and 199 isotopic ratios (**Table 3**), is interpreted as the crystallization age of the Tiquié magmatism. Individual ages vary from 1760 Ma to 1743 Ma. Only one crystal yielded a $^{207}Pb/^{206}Pb$ age of 2034 ± 2 Ma (**Figure 9b**) from 32 isotopic ratios (**Table 3**), interpreted as the protolith age of the Trairão and Anauá basements of the Tapajós-Parima Province.

Rhyodacite (EA-08 sample; Cachoeira do Machado Formation)

The EA-08 sample shows a zircon population with 80-240 µm variation in length, colorless to very pale yellow, transparent and bipyramidal, with discrete prismatic habit (length/width ratios 1.5:1 to 2:1), slightly corroded faces, rounded vertices. The zircons are also free-inclusions with local cracks. Six crystals with individual ages varying from 1756 Ma to 1747 Ma yielded a mean $^{207}Pb/^{206}Pb$ age of 1751 ± 2 Ma (MSWD: 1.8; **Figure 9d**), from 196 isotopic ratios (**Table 3**), interpreted as the crystallization age of the Cachoeira do Machado magmatism, coeval with ~1.75 Ga granitoids.

6.3 Whole-Rock Sm-Nd

T**able 4** shows three new WR Sm-Nd isotopic results for ~1.75 Ga granitoid rocks of the Rio Negro Province. Sm-Nd isotopic data were also compiled from Rio Negro (basement rocks) and Tapajós-Parima provinces to recognize suitable crustal sources (**Figure 10**). All analyzed samples show positive ε_{Nd} (+2.27 to +0.92) and T_{DM} ages varying from 2.01 Ga to 1.91 Ga (Figure 11), suggesting the contribution of depleted sources of Cauaburi basement or/and mantle/juvenile sources. The zircon population shows local inheritance from Tapajós-Parima Province (2034 Ma), however, the Sm-Nd data results exclude this basement as a source of the 1.75 granitoid rocks (**Figure 10**).

Table 3. Single zircon Pb-evaporation isotopic data for Marié-Mirim (EP-189), Marauiá (PV-38), and Tiquié (AF-338) Suites.

sample/grain number	Temp.(°C)	Number of ratios	$^{204}Pb/^{206}Pb$	2σ	$^{208}Pb/^{206}Pb$	2σ	$^{207}Pb/^{206}Pb$	2σ	$(^{207}Pb/^{206}Pb)_c$	2σ	age	2σ
Marié-Mirim Suite, Mirim-Mirim Granite, type-area												
EP-189/3	1450	36/36	0.000962	40	0.29138	93	0.12268	36	0.10983	43	1797	7
	**1500*	*0/8*	*0.000076*	*34*	*0.27892*	*144*	*0.11325*	*47*	*0.11222*	*66*	*1836*	*11*
EP-189/4	1500	8/8	0.000137	52	0.25669	226	0.11212	55	0.11026	90	1804	15
EP-189/8	*#1450*	*0/8*	*0.001011*	*68*	*0.27690*	*144*	*0.12270*	*88*	*0.10897*	*129*	*1782*	*22*
	1500	16/16	0.000055	7	0.22862	80	0.11163	24	0.11086	24	1814	4
EP-189/10	1500	28/28	0.000129	32	0.28780	153	0.11113	48	0.10953	42	1792	7
EP-189/12	1500	32/32	0.000123	8	0.25149	134	0.11181	25	0.11016	23	1802	4
		120 (136)					**USD 3.3**			**mean age**	**1805**	**8**
EP-189/5	1500	12/12	0.000744	116	0.23361	399	0.11760	245	0.10731	104	1755	18
EP-189/6	1450	38/38	0.001515	14	0.27420	154	0.12751	33	0.10692	31	1748	5
EP-189/9	1500	14/14	0.000246	2	0.24999	118	0.11142	84	0.10783	29	1763	5
		64 (64)					**USD 3.4**			**mean age**	**1756**	**12**
Marauiá Suite, Marauiá Granite, type-area												
PV-38/2	**1450*	*0/40*	*0.000109*	*4*	*0.08140*	*34*	*0.10436*	*15*	*0.10284*	*18*	*1703*	*3*
	1500	0/38	0.000018	2	0.11168	78	0.10882	26	0.10860	25	1780	4
	1550	18/18	0.000023	2	0.11649	83	0.10920	27	0.10888	27	1781	5
PV-38/4	**1450*	*0/36*	*0.000195*	*25*	*0.11055*	*67*	*0.10868*	*25*	*0.10586*	*43*	*1778*	*4*
	1500	28/28	0.000039	6	0.17046	41	0.11000	36	0.10930	30	1788	5
		46 (160)					**USD 2.6**			**mean age**	**1781**	**7**
PV-38/1	**1450*	*0/40*	*0.000124*	*5*	*0.06685*	*120*	*0.10539*	*18*	*0.10361*	*20*	*1690*	*4*
	1485	40/40	0.000052	4	0.10681	43	0.10756	19	0.10676	20	1745	3
	1510	18/18	0.000051	3	0.14098	184	0.10796	42	0.10730	51	1754	9
		58 (98)					**USD 2.1**			**mean age**	**1746**	**6**
PV-38/5	1450	38/38	0.000055	7	0.08351	25	0.10502	49	0.10437	47	1704	8
PV-38/8	1450	36/36	0.000159	53	0.08787	26	0.10684	28	0.10496	30	1714	5
	1500	38/38	0.000115	8	0.08735	20	0.10656	13	0.10506	19	1716	3
		112 (112)					**USD 1.9**			**mean age**	**1714**	**5**
PV-38/3	*1450	0/38	0.000120	6	0.06957	72	0.10299	33	0.10118	24	1646	4
	1500	26/26	0.000124	17	0.06800	18	0.10323	14	0.10157	18	1653	3
		26 (64)					**USD 2.6**			**mean age**	**1651**	**7**
Tiquié Suite, Tiquié Granite, type-area												
AF-338/10	**1500*	*0/34*	*0.000101*	*12*	*0.17439*	*126*	*0.12321*	*62*	*0.12197*	*53*	*1986*	*8*
	1530	32/32	0.000080	5	0.18760	45	0.12643	15	0.12536	15	2034	2
		32 (66)					**USD: 0.7**			**mean age**	**2034**	**2**
AF-338/1	**1450*	*0/34*	*0.000157*	*5*	*0.16707*	*70*	*0.10813*	*32*	*0.10617*	*51*	*1735*	*9*
	1500	40/40	0.000024	3	0.18452	96	0.10764	27	0.10726	33	1754	6
AF-338/2	**1450*	*0/40*	*0.000239*	*6*	*0.16927*	*142*	*0.10928*	*61*	*0.10619*	*52*	*1735*	*9*
	1500	08/08	0.000000	0	0.19578	96	0.10765	34	0.10765	34	1760	6
AF-338/4	*#1450*	*0/32*	*0.000835*	*16*	*0.19958*	*45*	*0.11760*	*27*	*0.10622*	*35*	*1736*	*6*
	1500	04/04	0.000051	22	0.19242	97	0.10744	267	0.10675	269	1745	46
AF-338/5	*#1450*	*0/32*	*0.001372*	*116*	*0.23256*	*108*	*0.12615*	*40*	*0.10766*	*133*	*1761*	*23*
	1500	30/30	0.000081	8	0.20953	125	0.10821	43	0.10703	37	1750	6
AF-338/6	1450	38/38	0.000225	14	0.21417	323	0.10951	19	0.10641	23	1739	4
AF-338/7	**1450*	*7/14*	*0.000344*	*4*	*0.20193*	*97*	*0.11116*	*27*	*0.10647*	*27*	*1740*	*5*
	1500	38/38	0.000146	32	0.19038	61	0.10849	39	0.10662	48	1743	8
AF-338/8	*#1450*	*0/28*	*0.001525*	*13*	*0.21338*	*211*	*0.12015*	*94*	*0.09891*	*131*	*1604*	*25*
	1500	34/34	0.000068	6	0.17931	117	0.10813	18	0.10719	28	1752	5
		199 (372)					**USD: 2.9**			**mean age**	**1747**	**6**
Cachoeira do Machado Formation, type-area (rhyodacite)												
EA08/1	1450	12/12	0.000110	25	0.17673	316	0.10689	24	0.10689	12	1747	4
EA08/3	1500	30/30	0.000089	3	0.13625	84	0.10706	31	0.10706	15	1750	5
EA08/6	1450	36/36	0.000228	11	0.18260	152	0.10721	26	0.10721	13	1753	5
	1500	30/30	0.000099	10	0.17851	80	0.10684	27	0.10684	13	1747	5
EA08/7	1500	24/24	0.000120	10	0.16706	52	0.10724	16	0.10724	8	1753	3
EA08/9	*#1450*	*0/34*	*0.000635*	*22*	*0.18307*	*146*	*0.10444*	*28*	*0.10444*	*14*	*1705*	*5*
	1500	38/38	0.000084	13	0.16831	85	0.10699	17	0.10699	9	1749	3
EA08/12	*#1450*	*0/6*	*0.001698*	*192*	*0.16196*	*706*	*0.10481*	*341*	*0.10480*	*171*	*1711*	*60*
	1500	26/26	0.000024	8	0.16512	187	0.10738	21	0.10738	10	1756	4
		196 (236)					**USD: 1.8**			**mean age**	**1751**	**2**

Notes: Crystal numbers are indicated. The column number of ratios shows the total of isotopic ratios used to the age calculation and, in parenthesis, the total isotopic ratios measured. Evaporation steps in italics were not included in the age calculation of each grain due to: * too much higher or lower values of the $^{207}Pb/^{206}Pb$ ratio in relation to the average of the zircon, and # $^{204}Pb/^{206}Pb$ > 0.0004.

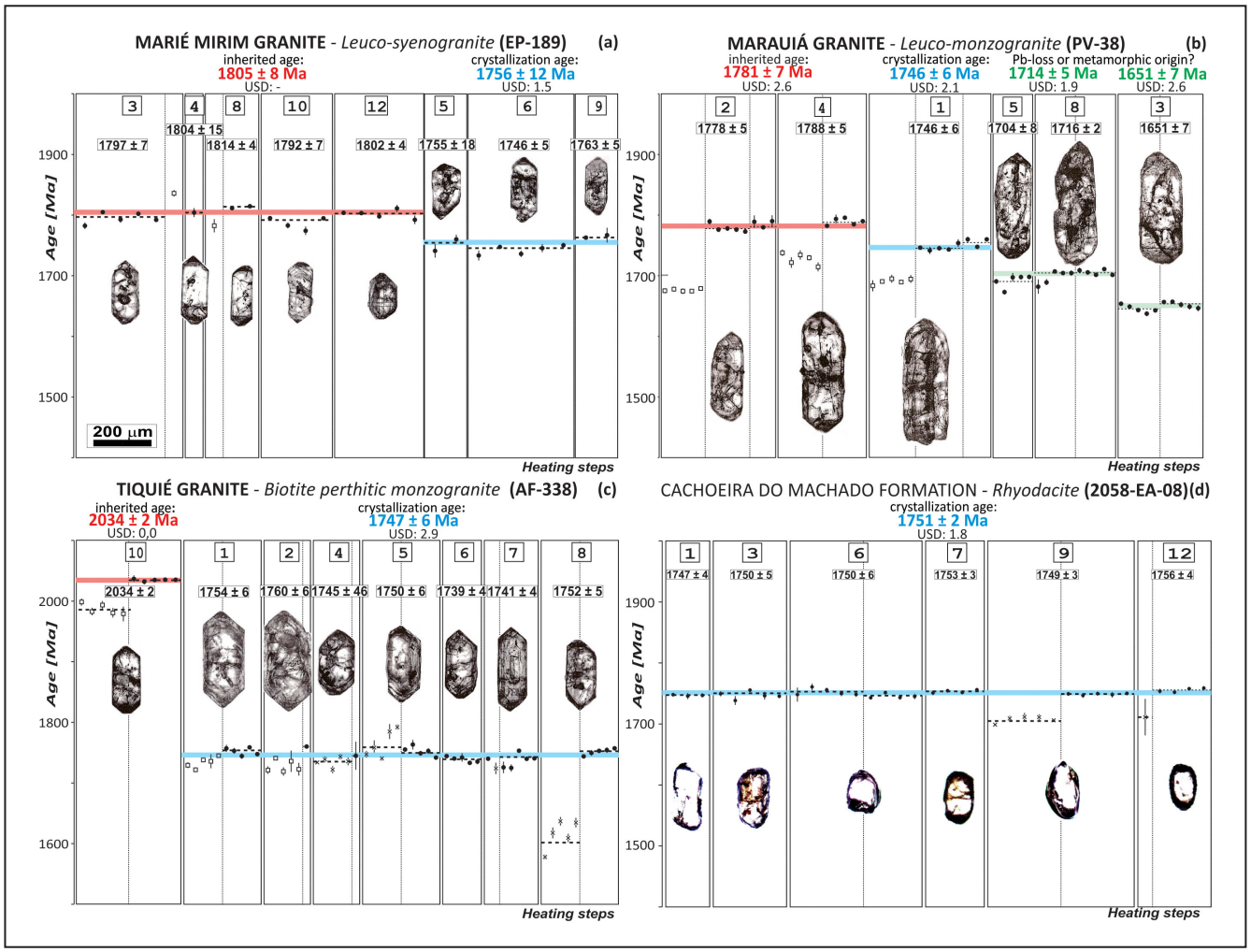

FIGURE 9. Single zircon Pb-evaporation ages for early Sthaterian A-type granites and coeval volcanic rocks: (a) Marié-Mirim (EP-189), (b) Marauiá (PV-38), (c) Tiquié (AF-338) suites and (d) Cachoeira do Machado Formation. Symbols: Filled circle - accepted blocks for age calculation, Square - blocks not used due to their higher or lower values of the $^{207}Pb/^{206}Pb$ ratio concerning the mean, X - rejected blocks due to $^{204}Pb/^{206}Pb > 0.0004$. Crystal numbers are indicated (see Table 3). The scale bar is the same for all diagrams.

TABLE 4. Nd isotopic data of ~1.75 Ga A-type and related rocks in the NW Amazon Craton.

sample	rock	Unit	T_{crist} (Ma)	ref	Sm (ppm)	Nd (ppm)	Sm/Nd	f(Sm/Nd)	$^{147}Sm/^{144}Nd$	$^{143}Nd/^{144}Nd$	$eNd_{(0)}$	$eNd_{(t)}$	$T_{(DM)}$	ref
EP-189	Leuco syenogranite	Marié-Mirim Suite (type-area)	1756	1	7.57	42.76	0.18	-0.51	0.095488	0.511562	-20.99	+2.27	1.91	1
AF-338	Microperthitic biotite monzogranite	Tiquié Suite (type-area)	1746	1	17.02	129.44	0.13	-0.50	0.098559	0.511572	-20.79	+1.76	1.95	1
PV-38	Leuco monzogranite	Marauiá Suite (type-area)	1746	1	6.90	42.32	0.16	-0.50	0.099212	0.511537	-21.48	+0.92	2.01	1

Nd T_{DM} ages are calculated using the model of De Paolo (1981) for Nd evolution of the depleted mantle; Obs: ea. estimated age. Ref. References: 1. This paper;

7. Discussion

7.1 Constraints on mineralizations, potential sources and petrogenetic models

The studied granitoids display low to moderate concentrations of REE (except Eu), high HFSE, Ga/Al*10000 (0.8-3.7), agpaitic index (0.9-1.2), and Fe-number (0.8-1.0). These features together with their alkaline/aluminous and ferroan nature classify the rocks as A-type within-plate granites, mainly the Marié-Mirim (peralkaline, alkalic/alkali-calcic) and Marauiá (peraluminous, alkalic-calcic/calc-alkaline) Suites, both located in the Northeastern Domain. Despite both granites displaying similar REE and incompatible element profiles, the Harker diagrams indicate their non-cogenetic nature.

Located in the Southwestern Domain, the Tiquié Suite shows transitional chemical characteristics among I-type to A-type (ambiguous granites ***sensu*** Whalen 2005), showing high HFSE values and Nb-Ta negative anomalies, including

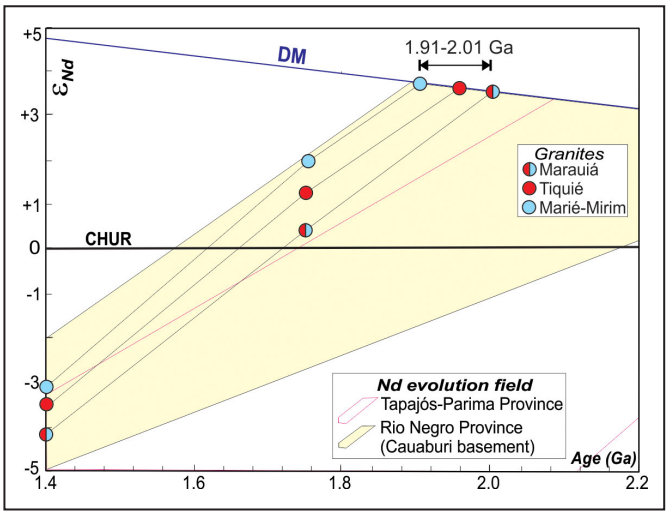

FIGURE 10. ε_{Nd} vs time diagram for ~1.75 Ga granites of NW Amazon Craton. The Nd evolution fields of previous data of the Cauaburi basement (Rio Negro Province) and Tapajós-Parima Province are plotted for comparison. Tc: crystallization age range. For details see text and table 4. The DM model adopted is based on DePaolo (1981). Nd data of the Tapajós-Parima Province: Sato and Tassinari (1997), Santos et al. (2000), Lamarão et al. (2005) and Almeida (2006); Nd data of the Cauaburi basement (Rio Negro Province): Almeida et al. (2022).

metaluminous, ferroan to magnesian and alkalic-calcic signatures. The "ambiguous" term (e.g. Whalen 2005, Bonin 2007) reinforces the lack of consensus about A-type magma origin, suggesting that the last one does not form a genetically connected group of rocks. Other authors (e.g. Creaser et al. 1991) have proposed that the term A-type should be abandoned, this being nothing more than a subtype of I-type (e.g. Collins et al. 1982).

According to Bettencourt et al. (2016), greisen and pegmatite-related Sn-Nb-Ta deposits in the Amazon Craton are preferentially related to late-orogenic to anorogenic A-type granites with 1.84 to 1.75 Ga, such as observed in the SE Amapá. The studied granites in the NW Amazon may be linked to the final stages of this mineralizing event (1.75 Ga), showing also A-type chemical affinity and the existence of veins, pegmatites, and greisens, suggesting a mineral potential for other rare metals (W, Mo, REE, etc.) and gemstones, in addition to the known occurrences of Sn-Nb-Ta. However, these rare-metal occurrences (Sn, W, Mo, REE) indicate a much more substantial participation of crustal or enriched components in the melt generation, contrasting with the Nd isotopic signature available for the Tiquié, Marauiá, and Marié-Mirim Suites.

All these felsic granites contain in different proportions dissolved OH–F-bearing fluids (e.g. fluorite, topaz), crystallizing under reduced (ilmenite) to oxidized (titanite, magnetite, quartz) conditions, with high temperatures (1205°C to 1085°C) and locally with coeval volcanism preserved (Cachoeira do Machado).The relatively oxidizing conditions (locally reduced), HFSE concentrations, and Nd isotope data (ε_{Nd} +2.27 to +0.92) favor derivation of these granitoid rocks from sources containing a large mantle input or from depleted source (Cauaburi basement?) contributions with 1.91 Ga to 2.01 Ga T_{DM} ages. For oxidized granites (e.g. Marauiá and Tiquié Suites), the magma origin involves partial melting of oxidized lower crustal quartz feldspathic igneous sources (e.g. Dall'Agnol and Oliveira 2007) or charnockite sources (e.g. Landenberger and Collins 1996, Zhao et al. 2008), these last ones mainly with HFSE chemical depletion.

According to Dall'Agnol and Oliveira (2007), reduced A-type granites (e.g. Marié-Mirim Suite) show at least three possibilities of sources (or combination of sources): (a) quartz feldspathic igneous sources with reduced character (Anderson and Morrison 2005); (b) local metasedimentary contribution (Dall'Agnol et al. 2005), or (c) origin by differentiated tholeiitic sources (e.g. Frost and Frost 1997, Frost et al. 1999).

7.2 Emplacement, Deformation, and Evolution Model for the ~1.75 Ga granites in NW Amazon Craton

A large long-lived magmatic arc (1840-1700 Ma) defining an accretionary process in the NW Amazon Craton was proposed by Almeida et al. (2022). According to these authors, a 1.81-1.76 Ga calc-alkaline basement rocks (Cauaburi Complex) was generated in a normal to mature continental arc system (early stages), involving mixed crustal-mantle sources, with northeastwards subduction beneath the Tapajós-Parima Province. Despite some differences (e.g. age intervals, source compositions, etc.), this subduction-accretionary model shows some similarities with previous models based only on geochronology data (1.8-1.7 Ga, Tassinari et al. 1996; 1800-1740 Ma "Atabapo Belt'', Cordani et al. 2016).

Almeida et al. (2022) suggest that ~1.75 Ga A-type granites were generated from the melting of depleted calc-alkaline basement associated with subduction-related underplating processes (Cauaburi Orogeny) based on slab break-off model in a post-collisional context (post-1.78 Ga collisional event). Although such a mechanism dominantly occurs in the within-plate setting, magma underplating shows the same importance for the crustal growth in some subduction-related settings, such as in the extensional active continental margin (e.g. Petford and Atherton 1996).

In the NW Amazon Craton (Colombia side), Bonilla et al (2021) indicate for these 1.75 Ga A-type granites (Tiquié-like) a syn-collisional origin, however this magmatism is related to the final of the Querari Orogeny evolution (1.75-1.70 Ga; Almeida et al., 2022), probably representing a syn-orogenic stage without collision observed. These granites also post-dated the metamorphic peak in the Cauaburi Orogeny (~1.78 Ga), considered here as post-collisional. This example shows that ferroan and SiO_2-rich granite (A-type) are not exclusive of anorogenic settings, and most of the time they constitute exceptions (e.g. King et al. 1997, Bonin, 2007, Hinchey et al. 2023).

Granites with mantle-like isotopic signatures, as the studied granites, suggest that transitional (e.g. Tiquié Suite; eNd +1.76) and aluminous A-type granite (e.g. Marauiá Suite, eNd +0.92) are most probably derived respectively from tonalite and charnockite (depleted) sources (e.g. King et al. 1997), both heated by large-scale magmatic underplating (e.g. Zhao et al. 2008) in an extensional active continental margin (e.g. back-arc settings?) or associated to post-collisional gravitational collapse (e.g. Hinchey et al. 2023). The alkaline A-type granites (e.g. Marié-Mirim Suite; eNd +2.27), may be produced from the differentiation of tholeiitic mafic sources (mantle-plume) with low contributions of crustal sources

(metasedimentary or/and quartz feldspathic igneous sources with reduced character).

The chemical and isotopic characteristics suggest that these granites were generated in the final stages (1.75 Ga) of the second phase of the Cauaburi Orogen (1.81-1.76 Ga), in an extensional back-arc setting associated with underplating processes (**Figure 11**), probably produced by the initial and continuous rollback of a north-northeastward subducting slab, preceding the slab break-off proposed by Almeida et al. (2022). Thus, magmatic underplating may induce the dehydration of the middle-low crust to form charnockite, producing in sequence, for example, aluminous A-type magmatism from partial melting of this source (e.g. Zhao et al. 2008). The orogen collapse by gravitational processes may also induce the ascent of mantle-derived magmas along deep extensional faults in the post-collisional setting, common in Paleoproteroic times (e.g. Kaur et al. 2006, Hinchey et al. 2023).

Regarding the granite emplacement and the post-magmatic deformation, the granites of the Northeastern and Southwestern domains show different patterns. The A-type granites of the Northeastern Domain show higher volumes of magma, stronger structural-controlled emplacement, elongated shapes, and locally concentrated deformation in shear zones under high strain rates, compatible with greenschist (Marié-Mirim) to epidote-amphibolite (e,g, Marauiá Suite) facies, probably related to D_{n+2} event (K´Mudku Shear Belt). In the Southwestern Domain the transitional granites occur in low volumes, subcircular shapes, emplacement at higher crustal levels (Tiquié Suite) with coeval volcanism (Cachoeira do Machado), deformed under lower strain rates and temperatures, compatible with low greenschist, probably related to D_{n+3} event (Traíra Shear Belt).

8. Conclusions

Based on the geological, geochemical, and isotopic results, the studied granites show the following features:

Marauiá and Marié-Mirim suites (Northeastern Domain) are peralkaline to peraluminous, ferroan, and alkalic to calc-alkaline, corresponding to chemical signatures compatible with A-type granites. These granites show also higher volumes of magma, deeper and structural-controlled emplacement, and elongated shapes, locally with concentrated deformation in shear zones under high strain rates (D_{n+2} event), compatible with greenschist to epidote-amphibolite facies (K´Mudku Shear Belt);

Tiquié Suite (Southwestern Domain) is metaluminous, ferroan to magnesian, alkalic-calcic, including Nb-Ta negative anomalies, showing transitional characteristics among I-type and A-type granites, could also be classified as “ambiguous” granites ***sensu*** Whalen (2005). This granitic suite occurs in low volumes, and subcircular shapes, with emplacement at higher crustal levels and coeval volcanism (Cachoeira do Machado Formation);

The São Jorge leucogneisses show similar chemical A-type characteristics, but are not cogenetic with the Marauiá, Marié-Mirim, and Tiquié granites, presenting different sources. Furthermore, the leucogneisses show at least three deformational events and higher PT metamorphic conditions, contrasting with the studied granites;

All the studied granitic suites contain dissolved OH–F-bearing fluids (e.g. fluorite), the oxidation state of magma ranging from reduced (Marié-Mirim Suite) to oxidized (Marauiá and Tiquié Suites) estimated conditions, enriched-SiO_2 (70-76%), showing also high HFSE concentrations and magmas with high temperatures (1205°C to 1085°C);

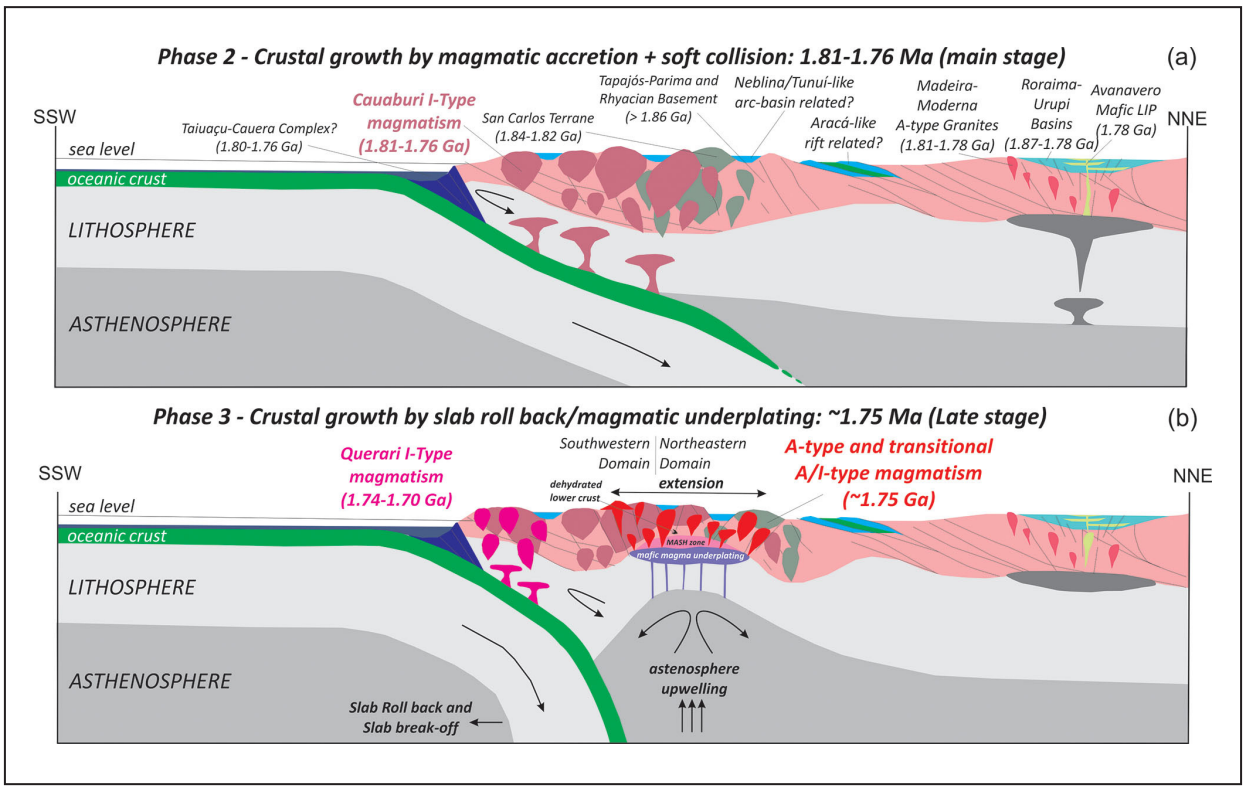

FIGURE 11. Schematic geodynamic model modified by Almeida et al. (2022) for (a) 1.81-1.76 Ga (2nd phase of Cauaburi Magmatic Arc) and (b) 1.75 Ga A-type and transitional A/I-type magmatism generation in the NW Amazon Craton.

The Nd isotope data (εNd +2.27 to +0.92) indicate derivation from depleted sources or sources containing a large mantle input. The magma origins could be involved partial melting of lower crustal quartz feldspathic igneous or charnockite sources (Tiquié and Marauiá Suites) and differentiation of tholeiitic mafic sources with low contributions of crustal sources (Marié-Mirim Suite), showing mineral potential for Sn, Ta, and Nb and probably for others rare metals and gemstones;

The chemical and isotopic signatures indicate that these granites were generated in the final stages (1.75 Ga) of the Cauaburi Orogen (1.81-1.76 Ga), related to an extensional back-arc (or gravitational collapse?) associated with large-scale magmatic underplating in the post-collisional setting. Thisprocess was probably produced by the initial and continuous rollback of a north-northeastward subducting slab beneath the Tapajós-Parima Province, reworking/ recycling juvenile crust and/or the uprising of mantle-derived magmas.

Acknowledgments

The authors are grateful to the Geological Survey of Brazil-CPRM and CNPq (CT-Amazônia 575490/2008-0; Universal 476601/2011-8) for the support and research grants. This research is part of the NA.19 – Pico da Neblina Project (1:1.000.000 sheet) carried out by the Geological Survey of Brazil-CPRM in partnership with the Geological Survey of Colombia. We are also very grateful to all indigenous communities and to field workers Gerson Tavares, José Carneiro, Luis Ramirez, Olício Ferreira, Oscar Brito, Valdemilton Gusmão, Valdir Nogueira and Teodoro Oliveira for their fundamental support. Finally, thank you very much to Lauro Cézar M. de Lira Santos (Federal University of Pernambuco), and one anonymous reviewer, for your constructive comments and suggestions that substantially improved the manuscript.

Authorship credits

Author	A	B	C	D	E	F
MEA	■	■	■	■	■	■
MJBM		■	■	■	■	
TAAM			■		■	
JOSS			■		■	

A - Study design/Conceptualization **B** - Investigation/Data acquisition
C - Data Interpretation/ Validation **D** - Writing
E - Review/Editing **F** - Supervision/Project administration

References

Almeida M.E. 1997. Petrografia e geoquímica de elementos maiores da Suíte Intrusiva Tiquié: o caso dos Granitos Tiquié e Marié-Mirim no estado do Amazonas. In: Costa M.L., Angélica R.S. (coord.). Contribuições à geologia da Amazônia. Belém, FINEP, SBG-NO, p. 122-145.

Almeida M.E. 2006. Evolução geológica da porção central do Escudo das Güianas com base no estudo geoquímico e isotópico dos granitóides paleoproterozóicos do sudeste de Roraima, Brasil. PhD Thesis, Instituto de Geociências, Universidade Federal do Pará, Belém, 226 p.

Almeida M.E., Fraga L.M.B., Brito M.F.L., Santos C.A., Silva M.A., Gomes H.A., Larizzatti J.H., Giovannini C.A., Villas Boas P.F., Luzardo R., Silva L.C. 2000. Serra Imeri: folhas NA.20-Y/SA.20-V e SA.20-V-B. Estado do Amazonas. Manaus, CPRM, 1 CD-ROM.

Almeida M.E., Larizzatti J.H. 1996a. Geologia e petrografia, dos gnaisses migmatíticos do alto Rio Uaupés, estado do Amazonas, Brasil. In: Congresso Brasileiro de Geologia, 39, v. 6, 293-296.

Almeida M.E., Larizzatti J.H. 1996b. Geologia e petrografia da Suíte Intrusiva Içana no alto Rio Uaupés, estado do Amazonas, Brasil. In: Congresso Brasileiro de Geologia, 39, v. 6, 399-403.

Almeida M.E., Macambira M.J.B., Santos J.O.S., Nascimento R.S.C., Paquette J.L., Vasconcelos P., Luzardo R. 2011. A new geodynamic model for the Northwestern Amazon Craton (Amazonas, Brazil) based on field geology, geochemistry and geochronology data. In: Congresso Latino-Americano de Geologia, 14.

Almeida M.E, Nascimento R.S.C., Mendes T.A., Santos J.O.S., Macambira M.J.B., Vasconcelos P., Pinheiro S.S. 2022. An outline of Paleoproterozoic-Mesoproterozoic crustal evolution of the NW Amazon Craton and implications for the Columbia Supercontinent. International Geology Review, 64(22), 3195-3229. https://doi.org/10.1080/00206814.2021.2025158

Amaral G. 1974. Geologia Pré-Cambriana da região amazônica. Habilitation Thesis, Instituto de Geociências, Universidade de São Paulo, São Paulo, 212 p.

Anderson J.L., Bender E.E. 1989. Nature and origin of Proterozoic A-type granitic magmatism in the southwestern United States of America. Lithos, 23(1-2), 19-52. https://doi.org/10.1016/0024-4937(89)90021-2

Anderson J.L., Morrison J. 2005. Ilmenite, magnetite, and peraluminous Mesoproterozoic anorogenic granites of Laurentia and Baltica. Lithos, 80(1-4), 45-60. https://doi.org/10.1016/j.lithos.2004.05.008

Ansdell K.M., Kyser T.K. 1991. Plutonism, deformation and metamorphism in the Proterozoic Flin Flon greenstone belt, Canada: limits on timing provided by the single-zircon Pb-evaporation technique. Geology, 19(5), 518-521. https://doi.org/10.1130/0091-7613(1991)019%3C0518:PDAMIT%3E2.3.CO;2

Batchelor R.A., Bowden P. 1985. Petrogenetic interpretation of granitoid rock series using multicationic parameters. Chemical Geology, 48(1-4), 43-55. https://doi.org/10.1016/0009-2541(85)90034-8

Bettencourt J.S., Juliani C., Xavier R.P., Monteiro L.V.S., Bastos Neto A.C., Klein E.L., Assis R.R., Leite Jr. W.B., Moreto C.P.N., Fernandes C.M.D., Pereira V.P. 2016. Metallogenetic systems associated with granitoid magmatism in the Amazonian Craton: an overview of the present level of understanding and exploration significance. Journal of South American Earth Sciences, 68, 22-49. http://dx.doi.org/10.1016/j.jsames.2015.11.014

Bizzi L.A., Schobbenhaus C., Gonçalves J.H., Baars F.J., Delgado I.M., Abram M.B., Leão Neto R., Matos G.M.M., Santos J.O.S. Geologia, tectônica e recursos minerais do Brasil: Sistema de Informações Geográficas - SIG. Brasília, CPRM, 2004. 4 CD-ROMs.

Bonilla A., Cramer T., De Grave J., Alessio B., Glorie S., Kroonenberg S. 2021. The NW Amazonian Craton in Guainía and Vaupés departments, Colombia: transition between orogenic to anorogenic environments during the Paleo-Mesoproterozoic. Precambrian Research, 360, 106223. https://doi.org/10.1016/j.precamres.2021.106223

Bonin B. 2007. A-type granites and related rocks: evolution of a concept, problems and prospects. Lithos, 97(1-2), 1-29. https://doi.org/10.1016/j.lithos.2006.12.007

Bonin B., Janoušek V., Moyen J.-F. 2020. Chemical variation, modal composition and classification of granitoids. In: Janoušek V., Bonin B., Collins W.J., Farina F., Bowden P. (ed.). Post-Archean granitic rocks: petrogenetic processes and tectonic environments. Special Publication, 491. London, Geological Society, p. 9-51. https://doi.org/10.1144/SP491-2019-138

Boynton W.V. 1984. Cosmochemistry of the rare earth elements: meteorite studies. In: Henderson, P. (ed.). Rare earth element geochemistry. Amsterdam, Elsevier, p. 63-114.

Brown G.C., Thorpe R.S., Webb P.C. 1984. The geochemical characteristics of granitoids in contrasting arcs and comments on magma sources. Journal of the Geological Society, 141(3), 413-426. https://doi.org/10.1144/gsjgs.141.3.0413

Carneiro M.C.R., Nascimento R.S.C., Almeida M.E., Salazar C.A., Trindade I.R., Rodrigues V.O., Passos M.S. 2017. The Cauaburi Magmatic Arc: litho-stratigraphic review and evolution of the Imeri Domain, Rio Negro Province, Amazonas Craton. Journal of South American Earth Sciences, 77, 310-326. https://doi.org/10.1016/j.jsames.2017.06.001

Cawood P.A., Hawkesworth C.J. 2015. Temporal relations between mineral deposits and global tectonic cycles. In: Jenkin G.R.T., Lusty P.A.J., McDonald I., Smith M.P., Boyce A.J., Wilkinson J.J. (ed.). Ore deposits in an evolving Earth. Special Publications, 393. London, Geological Society, p. 9-21. https://doi.org/10.1144/SP393.1

Chapman J.B., Shields J.E., Ducea M.N., Paterson S.R., Attia S., Ardill K.E. 2021. The causes of continental arc flare ups and drivers of episodic magmatic activity in Cordilleran orogenic systems. Lithos, 398-399, 106307. https://doi.org/10.1016/j.lithos.2021.106307

Collins W.J., Beams S.D., White A.J.R., Chappell B.W. 1982. Nature and origin of A-type granites with particular reference to southeastern Australia. Contributions to Mineralogy and Petrology, 80, 189-200. https://doi.org/10.1007/BF00374895

Cordani U.G., Sato K., Sproessner W, Fernandes F.S. 2016. U-Pb zircon ages of rocks from the Amazonas territory of Colombia and their bearing on the tectonic history of the NW sector of the Amazonian Craton. Brazilian Journal of Geology, 46(supl. 1), 5-35. https://doi.org/10.1590/2317-4889201620150012

Cordani U.G., Tassinari C.C.G., Teixeira W., Basei M.A.S., Kawashita K. 1979. Evolução tectônica da Amazônia com base nos dados geocronológicos. In: Congresso Geológico Chileno, 2, v. 4, 177-148.

Creaser R.A., Price R.C., Wormald R.J. 1991. A-type granites revisited: assessment of a residual-source model. Geology, 19(2), 163-166. https://doi.org/10.1130/0091-7613(1991)019%3C0163:ATGRAO%3E2.3.CO;2

Dall'Agnol R., Macambira M.J.B. 1992. Titanita-biotita granitos do Baixo Rio Uaupés, Província Rio Negro, Amazonas. Parte I: geologia, petrografia e geocronologia. Revista Brasileira de Geociências, 22(1), 3-14. Available online at: http://bjg.siteoficial.ws/1992/n.1/1.pdf / (accessed on 23 Nov. 2023).

Dall'Agnol R., Oliveira D.C. 2007. Oxidized, magnetite-series, rapakivi-type granites of Carajás, Brazil: implications for classification and petrogenesis of A-type granites. Lithos, 93(3-4), 215-233. https://doi.org/10.1016/j.lithos.2006.03.065

Dall'Agnol R., Teixeira N.P., Rämö O. T., Moura C.A.V., Macambira M.J.B., Oliveira D.C. 2005. Petrogenesis of the Paleoproterozoic rapakivi A-type granites of the Archean Carajás metallogenic province, Brazil. Lithos, 80(1-4), 101-129. https://doi.org/10.1016/j.lithos.2004.03.058

Daneshvar N., Azizi H., Tsuboi M. 2022. Estimating magma crystallization temperatures using high field strength elements in igneous rocks. Minerals, 12(10), 1260. https://doi.org/10.3390/min12101260

De la Roche H., Leterrier J., Grandclaude P., Marchal M. 1980. A classification of volcanic and plutonic rocks using R1R2-diagram and major-element analyses - its relationships with current nomenclature. Chemical Geology, 29(1-4), 183-210. https://doi.org/10.1016/0009-2541(80)90020-0

DePaolo D.J. 1981. Neodymium isotopes in the Colorado Front Range and crust-mantle evolution in the Proterozoic. Nature, 291(5812), 193-196. https://doi.org/10.1038/291193a0

Dougherty-Page J.S., Bartlett J.M. 1999. New analytical procedures to increase the resolution of zircon geochronology by the evaporation technique. Chemical Geology, 153(1-4), 227-240. https://doi.org/10.1016/S0009-2541(98)00158-2

Eby G.N. 1990. The A-type granitoids: a review of their occurrence and chemical characteristics and speculations on their petrogenesis. Lithos, 26(1-2), 115-134. https://doi.org/10.1016/0024-4937(90)90043-Z

Eby G.N. 1992. Chemical subdivision of the A-type granitoids: petrogenetic and tectonic implications. Geology, 20(7), 641-644. https://doi.org/10.1130/0091-7613(1992)020%3C0641:CSOTAT%3E2.3.CO;2

FuYuan W., XiaoChi L., WeiQiang J., JiaMin W., Lei Y. 2017. Highly fractionated granites: recognition and research. Science China Earth Sciences, 60(7), 1201-1219. https://doi.org/10.1007/s11430-016-5139-1

Frost C.D., Frost B.R. 1997. Reduced rapakivi-type granites: the tholeiite connection. Geology, 25(7), 647-650. https://doi.org/10.1130/0091-7613(1997)025%3C0647:RRTGTT%3E2.3.CO;2

Frost C.D., Frost B.R., Chamberlain K.R., Edwards B.R. 1999. Petrogenesis of the 1.43 Ga Sherman batholith, SE Wyoming, USA: a reduced, rapakivi-type anorogenic granite. Journal of Petrology, 40(12), 1771-1802. https://doi.org/10.1093/petroj/40.12.1771

Frost B.R., Barnes C.G., Collins W.J., Arculus R.J., Ellis D.J., Frost C.D. 2001. A geochemical classification for granitic rocks. Journal of Petrology, 42(11), 2033-2048. https://doi.org/10.1093/petrology/42.11.2033

Frost C.D., Frost B.R. 2011. On ferroan (A-type) granitoids: their compositional variability and modes of origin. Journal of Petrology, 52(1), p. 39-53. https://doi.org/10.1093/petrology/egq070

Frost C.D., Frost B.R. 2013. Proterozoic ferroan feldspathic magmatism. Precambrian Research, 228, 151-163. https://doi.org/10.1016/j.precamres.2013.01 .016

Gaudette H.E., Lafon J.M., Macambira M.J.B., Moura C.A.V., Scheller T. 1998. Comparison of single filament Pb evaporation/ionization zircon ages with conventional U-Pb results: examples from the Precambrian of Brazil. Journal of South American Earth Sciences, 11(4), 351-363. https://doi.org/10.1016/S0895-9811(98)00019-4

Gibbs A.K., Barron C.N. 1993. The geology of the Guyana Shield. Oxford, Oxford University Press, 245 p.

Hackley P.H., Urbani F., Karlsen A.W., Garrity C.P. 2006. Geologic shaded relief map of Venezuela. Open-File Report 2005-1038. Reston, VA, U.S. Geological Survey, 2 sheets. https://doi.org/10.3133/ofr20051038

Hawkesworth C.J., Cawood P.A., Dhuime B. 2016. Tectonics and crustal evolution. GSA Today, 26(9), 4-11. https://doi.org/10.1130/GSATG272A.1

Hildreth W., Moorbath S. 1988. Crustal contributions to arc magmatism in the Andes of Central Chile. Contributions to Mineralogy and Petrology, 98(4), 455-489. https://doi.org/10.1007/BF00372365

Hinchey A.M., Sandeman H.A., Butler J.P. 2023. The Paleoproterozoic granite factory: voluminous post-collisional, ferroan, A-type granites and implications for crust formation and metallogenic tenor, Labrador, Canada. GSA Bulletin. https://doi.org/10.1130/B36727.1

Hoffman A.W. 1988. Chemical differentiation of the Earth: the relationship between mantle, continental crust, and oceanic crust. Earth and Planetary Science Letters, 90(3), 297-314. https://doi.org/10.1016/0012-821X(88)90132-X

Irvine T.N., Baragar W.R.A. 1971. A guide to the chemical classification of the common volcanic rocks. Canadian Journal of Earth Sciences, 8(2), 523-548. https://doi.org/10.1139/e71-055

Janoušek V., Bonin B., Collins W.J., Farina F., Bowden P. 2020. Post-Archean granitic rocks: contrasting petrogenetic processes and tectonic environments. In: Janoušek V., Bonin B., Collins W.J., Farina F., Bowden P. (ed.). Post-Archean granitic rocks: petrogenetic processes and tectonic environments. Special Publication, 491. London, Geological Society, p. 1-8. https://doi.org/10.1144/SP491-2019-197

Johansson A. 2023. A tentative model for the origin of A-type granitoids. Minerals, 13(2), 236. https://doi.org/10.3390/min13020236

Kaur P., Chaudhri N., Raczek I., Kröner A., Hofmann A.W. 2006. Geochemistry, zircon ages and whole-rock Nd isotopic systematics for Palaeoproterozoic A-type granitoids in the northern part of the Delhi belt, Rajasthan, NW India: implications for late Palaeoproterozoic crustal evolution of the Aravalli craton. Geological Magazine, 144(2), 361-378. https://doi.org/10.1017/S0016756806002950

King P.L., White A.J.R., Chappell B.W., Allen C.M. 1997. Characterization and origin of the aluminous A-type granites of the Lachlan Fold Belt, southeastern Australia. Journal of Petrology, 38(3), 371-391. https://doi.org/10.1093/petroj/38.3.371

Kober B. 1986. Whole-grain evaporation for $^{207}Pb/^{206}Pb$-age-investigations on single zircons using a double-filament thermal ion source. Contributions to Mineralogy and Petrology, 93(4), 482-490. https://doi.org/10.1007/BF00371718

Kober B. 1987. Single-zircon evaporation combined with Pb^+ emitter bedding for $^{207}Pb/^{206}Pb$-age investigations using thermal ion mass spectrometry, and implications for zirconology. Contributions to Mineralogy and Petrology, 96(1), 63-71. https://doi.org/10.1007/BF00375526

Lamarão C.N., Dall'Agnol R., Pimentel M.M. 2005. Nd Isotopic composition of Paleoproterozoic volcanic and granitoid rocks of Vila Riozinho: implications for the crustal evolution of the Tapajós Gold Province, Amazon craton. Journal of South American Earth Sciences, 18(3-4), 277-292. https://doi.org/10.1016/j.jsames.2004.11.005

Landenberger B., Collins W.J. 1996. Derivation of A-type granites from a dehydrated Charnockitic lower crust: evidence from the Chaelundi Complex, eastern Australia. Journal of Petrology, 37(1), 145-170. https://doi.org/10.1093/petrology/37.1.145

Le Maitre R.W. 1976. The chemical variability of some common igneous rocks. Journal of Petrology, 17(4), 589-598. https://doi.org/10.1093/petrology/17.4.589

Lima M.I.C., Pires J.L. 1985. Geologia da região do Alto Rio Negro - AM. In: Simpósio de Geologia da Amazônia, 2, 140-154.

Loiselle M.C., Wones D.R. 1979. Characteristics and origin of anorogenic granites. Geological Society of America Abstracts with Programs, 12(7), 468.

Macambira M.J.B., Teixeira W., Vasquez M.L. 2020. O Cráton Amazônico e suas províncias geocronológicas: o legado de Umberto Cordani. In: Bartorelli A., Teixeira W., Brito Neves B.B. (org.). Geocronologia e evolução tectônica do Continente Sul-Americano: a contribuição de Umberto Giuseppe Cordani. São Paulo, Solaris Edições Culturais, p. 47-62.

Melo A.F.F., Villas Boas P.F. (org.). 1993. Projeto Alto Rio Negro: relatório preliminar. Manaus, CPRM. Available online at: https://rigeo.sgb.gov.br/jspui/handle/doc/8473 / (accessed on 10 Nov. 2023).

Mendes T.A.A., Mesquita R.B., Almeida M.E. 2020. Mapa geológico área Tunuí-Caparro folhas NA.19-Z-A-II, NA.19-Z-A-V e NA.19-Z-A-VI. Escala 1:250.000. Manaus, SGB-CPRM. Available online at: https://rigeo.sgb.gov.br/jspui/handle/doc/21745 / (accessed on 10 Nov. 2023).

Mendes T.A.A., Mesquita R.B., Knauer L.G., Almeida M.E., Roncato J. 2021. Spatiotemporal constraints on the western Cauaburi Belt tectonics - northwestern Amazon Craton, Brazil. International Geology Review, 63(11), 1342-1365. https://doi.org/10.1080/00206814.2020.1768441

Mendoza V. 1972. Geología del area del rio Suapure: parte noroccidental del escudo de Guyana, Estado Bolivar, Venezuela. Conferencia Geológica Inter-Guayanas, 9, v. 6, 306-338.

Nardi L.V.S. 1991. Caracterização petrográfica e geoquímica dos granitos metaluminosos da associação alcalina: revisão. Pesquisas em Geociências, 18(1), 44-57. https://doi.org/10.22456/1807-9806.21361

Pearce J.A. 1996. Sources and settings of granitic rocks. Episodes, 19(4), 120-125. https://doi.org/10.18814/epiiugs/1996/v19i4/005

Pearce J.A., Harris N.B.W., Tindle A.G. 1984. Trace element discrimination diagrams for the tectonic interpretation of granitic rocks. Journal of Petrology, 25(4), 956-983. https://doi.org/10.1093/petrology/25.4.956

Petford N., Atherton M. 1996. Na-rich partial melts from newly underplated basaltic crust: the Cordillera Blanca Batholith, Peru. Journal of Petrology, 37(6), 1491-1521. https://doi.org/10.1093/petrology/37.6.1491

Pinheiro S.S., Fernandes P.E.C.A., Pereira E.R., Vasconcelos E.G., Pinto A.C., Montalvão R.M.G., Issler R.S., Dall'Agnol R., Teixeira W., Fernandes C.A.C. 1976. Geologia. In: DNPM. Folha NA.19 Pico da Neblina: geologia, geomorfologia, pedologia, vegetação, uso potencial da terra. Projeto RADAMBRASIL. Rio de Janeiro, p. 17-137. Available online at: https://biblioteca.ibge.gov.br/visualizacao/livros/liv24028.pdf / (accessed on 13 Nov. 2023).

Pirajno F., Santosh M. 2015. Mantle plumes, supercontinents, intracontinental rifting and mineral systems. Precambrian Research, v. 259, 243-261. https://doi.org/10.1016/j.precamres.2014.12.016

Reis N.J., Almeida M.E., Ferreira A.L., Riker S.L. (org.). 2006. Geologia e recursos minerais do estado do Amazonas. Manaus, CPRM, CIAMA. Available online at: https://rigeo.sgb.gov.br/handle/doc/2967 / (accessed on 13 Nov. 2023).

Reis N.J., Cordani U.G., Goulart L.E.A., Almeida M.E., Oliveira V., Maurer V.C., Wahnfried I. 2021. Zircon U-Pb SHRIMP ages of the Demêni-Mocidade Domain, Roraima, southern Guiana Shield, Brazil: extension of the Uatumã Silicic Large Igneous Province. Journal of the Geological Survey of Brazil, 4(1), 61-76. https://doi.org/10.29396/jgsb.2021.v4.n1.4

Rodrigues V.O. 2016. Evolução petrogenética e metamorfismo das rochas ortoderivadas da litofácies tarsira no perfil entre São Gabriel da Cachoeira e Cucuí - Amazonas. MSc Dissertation, Instituto de Ciências Exatas, Universidade Federal do Amazonas, Manaus, 65 p. Available online at: https://tede.ufam.edu.br/handle/tede/5501 / (accessed on 23 Nov. 2023).

Santos J.O.S., Hartmann L.A., Gaudette H.E., Groves D.I., McNaughton N.J., Fletcher I.R. 2000. A new understanding of the provinces of the Amazon Craton based on integration of field mapping and U-Pb and Sm-Nd geochronology. Gondwana Research, 3(4), 453-488. https://doi.org/10.1016/S1342-937X(05)70755-3

Santos J.O.S., Faria M.S., Riker S.R., Souza M.M., Hartmann L.A., Almeida M.E., McNaughton N.J., Fletcher I.R. 2006a. A faixa colisional K'Mudku (idade Grenvilliana) no norte do Cráton Amazonas: reflexo intracontinental do Orógeno Sunsás na margem ocidental do cráton. In: Simpósio de Geologia da Amazônia, 9, p. 160-163.

Santos J.O.S., Hartmann L.A., Faria M.S., Riker S.R., Souza M.M., Almeida M.E., McNaughton N.J. 2006b. A compartimentação do Cráton Amazonas em províncias: avanços ocorridos no período 2000-2006. In: Simpósio de Geologia da Amazônia, 9, p. 156-159.

Santosh M., Tsunogae T., Yang C.-X., Han Y.-S., Hari K.R., Prasanth M.P.M., Uthup S. 2020. The Bastar Craton, central India: a window to Archean-Paleoproterozoic crustal evolution. Gondwana Research, 79, 157-184. https://doi.org/10.1016/j.gr.2019.09.012

Sato K., Tassinari C.C.G. 1997. Principais eventos de acreção continental no Cráton Amazônico baseados em idade modelo Sm-Nd, calculada em evoluções de estágio único e estágio duplo. In: Costa M.L., Angélica R.S. (coord.). Contribuições à geologia da Amazônia. Belém, FINEP, Sociedade Brasileira de Geologia, v.1, p. 91-142. Available online at: http://arquivos.sbg-no.org.br/BASES/CGA%201.pdf / (accessed on 23 Nov. 2023).

Siivola J., Schmid R. 2007. A systematic nomenclature for metamorphic rocks: 12. List of mineral abbreviations. Recommendations by the IUGS Subcommission on the Systematics of Metamorphic Rocks. Beijing, IUGS.

Söderlund U. 1996. Conventional U-Pb dating versus single-grain Pb evaporation dating of complex zircons from a pegmatite in the high-grade gneisses of southwestern Sweden. Lithos, 38(1-2), 93-105. https://doi.org/10.1016/0024-4937(95)00042-9

Stacey J.S., Kramers J.D. 1975. Approximation of terrestrial lead isotope evolution by a two-stage model. Earth and Planetary Science Letters, 26(2), 207-221. https://doi.org/10.1016/0012-821X(75)90088-6

Tapias J.G., Meléndez M.F.A. (ed.). Compilando la geologia de Colombia: una visión a 2015. Bogotá, Servicio Geológico Colombiano, 429 p. Available online at: https://www2.sgc.gov.co/MGC/Paginas/pev33.aspx / (accessed on 23 Nov. 2023).

Tassinari C.C.G. 1981. Evolução tectônica da Província Rio Negro-Juruena na região Amazônica. MSc Dissertation, Instituto de Geocências, Universidade de São Paulo, São Paulo, 2 v., 99 p. https://doi.org/10.11606/D.44.1981.tde-11062013-163626

Tassinari C.C.G., Macambira M.J.B. 1999. Geochronological provinces of the Amazonian Craton. Episodes, 22 (3), 174-182. https://doi.org/10.18814/epiiugs/1999/v22i3/004

Tassinari C.C.G., Macambira M.J.B. 2004. A evolução tectônica do Cráton Amazônico. In: Mantesso-Neto V., Bartoreli A., Carneiro C.D.R., Brito-Neves B.B. (ed.). Geologia do Continente Sul-Americano: evolução da obra de Fernando Flávio Marques de Almeida. São Paulo, Beca, p. 471-485.

Tassinari C.C.G., Cordani U.G., Nutman A.P., Van Schmus W.R., Bettencourt J.S., Taylor P.N. 1996. Geochronological systematics on basement rocks from the Rio Negro-Juruena Province (Amazonian Craton) and tectonic implications. International Geology Review, 38(2), 161-175. https://doi.org/10.1080/00206819709465329

Teixeira W., Tassinari C.C.G., Cordani U.G., Kawashita K. 1989. A review of the geochronology of the Amazonian Craton: tectonic implications. Precambrian Research, 42(3-4), 213-227. https://doi.org/10.1016/0301-9268(89)90012-0

Thieblèmont D., Tégyey M. 1994. Une discrimination géochimique des roches différenciées témoin de la diversité d'origine et de situation tectonique des magmas calco-alcalins. Comptes Rendus de l'Académie des Sciences. Sciences de la Terre et des Planètes, série II, tome 319(1), 87-94. Available online at: https://gallica.bnf.fr/ark:/12148/bpt6k6244307z/f43.item / (accessed on 17 Nov. 2023).

Veras R.S., Nascimento R.S.C., Almeida M.E., Paquette J.-L., Carneiro M.C.R. 2018. Paleoproterozoic basement of Içana Domain, Rio Negro Province, northwestern Amazonian Craton: geology, geochemistry and geochronology (U-Pb and Sm-Nd). Journal of South American Earth Sciences, 86, 384-409. https://doi.org/10.1016/j.jsames.2018.07.003

Whalen J.B. 2005. A-type granites: >25 years later. Geochimica et Cosmochimica Acta, 69(10, Supl.), A84. Abstracts of the 15th Annual V.M. Goldschmidt Conference, Moscow, Idaho, May 2005.

Whalen J.B., Currie K.L., Chappell B.W. 1987. A-type granites: geochemical characteristics, discrimination and petrogenesis. Contributions to Mineralogy and Petrology, 95, 407-419. https://doi.org/10.1007/BF00402202

White A.J.R., Chappell B.W. 1983. Granitoid types and their distribution in the Lachlan Fold Belt, southeastern Australia. In: Roddick J.A. Circum-Pacific plutonic terranes. GSA Memoirs, 159. Boulder, CO, Geological Society of America, 21-34. https://doi.org/10.1130/MEM159-p21

Wood D.A., Tarney J., Varet J., Saunders A.D., Bougault H., Joron J.L., Treuil M., Cann J.R. 1979. Geochemistry of basalts drilled in the North Atlantic by IPOD Leg 49: implications for mantle heterogeneity. Earth and Planetary Science Letters, 42(1), 77-97. https://doi.org/10.1016/0012-821X(79)90192-4

Wynn J.C., Cox D.P., Gray F., Schruben P.G. (comp.). 1993. Geologic and tectonic map of the Venezuelan Guayana Shield. In: U.S. Geological Survey, Corporación Venezolana de Guayana. Geology and mineral resource assessment of the Venezuelan Guayana Shield. Geological Survey Bulletin 2062. Reston, VA, U.S. Geological Survey, p. 123. Available online at: https://pubs.usgs.gov/publication/b2062 / (accessed on 23 Nov. 2023).

Zhao X.-F., Zhou M.-F., Li J.-W., Wu F.-Y. 2008. Association of Neoproterozoic A- and I-type granites in South China: implications for generation of A-type granites in a subduction-related environment. Chemical Geology, 257(1-2), 1-15. https://doi.org/10.1016/j.chemgeo.2008.07.018